THE JOURNAL OF PHYSICAL CHEMISTRY C
A JOURNAL OF THE AMERICAN CHEMICAL SOCIETY

pubs.acs.org/JPCC
Article

Complementary and Spatially Resolved *Operando* Spectroscopic Investigation of Pt/Al_2O_3 and Pt/CeO_2 Catalysts during CO/NO Conversion

Daria Gashnikova,[#] Samuel Struzek,[#] Florian Maurer, Miriam R. Bauer, Carina B. Maliakkal, Christian Kübel, Maria Casapu, and Jan-Dierk Grunwaldt*

Cite This: https://doi.org/10.1021/acs.jpcc.5c01963
Read Online

ACCESS | Metrics & More | Article Recommendations | Supporting Information

ABSTRACT: The composition of reaction mixtures strongly influences the structural evolution and performance of noble metal-based catalysts. In this work, we compared the effect of the simultaneous presence of CO and NO on the noble metal state and CO oxidation activity of Pt/Al_2O_3 and Pt/CeO_2 catalysts under close-to-stoichiometric conditions using complementary *in situ*/*operando* X-ray and infrared spectroscopic techniques. For the utilized catalysts, the integral catalytic performance data indicated a diminished CO oxidation activity in the presence of NO, which is due to a competitive adsorption of CO and NO, as elucidated by the diffuse reflectance infrared Fourier transform spectroscopy and high-energy resolution X-ray fluorescence X-ray absorption near-edge structure results. Spatially resolved *operando* X-ray absorption spectroscopy investigations and extended X-ray absorption fine structure analysis unraveled that the addition of NO led to a higher oxidation state of Pt along the entire catalyst bed for both samples. Moreover, NO was found to delay the reduction of Pt particles on Al_2O_3 and hinder the formation of active Pt clusters on CeO_2. As a result, a more oxidized Pt state at the beginning of the catalyst bed and a low overall activity were observed for Pt/CeO_2. However, the CO oxidation activity could be enhanced by a reductive pretreatment of the Pt/CeO_2 catalyst, resulting in a similar reduced Pt state along the entire catalyst bed and minimizing the negative impact of NO during the combined reaction.

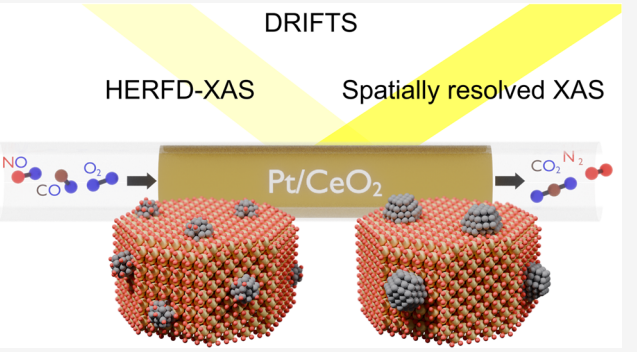

INTRODUCTION

The combustion of traditional and synthetic fuels for energy production leads to emissions of various air pollutants like CO, NO_x, and hydrocarbons that cause photochemical smog, acid rain, global warming, and health hazards for humans.[1,2] Noble metal catalysts are key materials for the reduction of such emissions from stationary and mobile sources,[3−7] as well as for the generation of green hydrogen[8,9] or the production of fine chemicals.[10,11] One of the most relevant applications in emission control remains the simultaneous removal of NO_x, CO, and hydrocarbons under stoichiometric conditions over Pt, Pd and/or Rh containing three-way catalysts. Hereby, CO and hydrocarbons are oxidized with O_2 to CO_2 and H_2O, while NO_x is reduced to nitrogen by CO or hydrocarbons.[5] Rh is typically used for the reduction of NO_x due to its outstanding NO dissociation ability, but the high costs of Rh demand cheaper alternatives. In this regard, Pt was found to be active for the NO_x reduction by CO,[12] and could be potentially used to at least partially replace Rh.

For Pt-based catalysts, previous studies have been mostly focused on unraveling the reaction mechanism of NO reduction by CO.[13] According to the literature, the mechanism is generally assumed to involve the nondissociative CO and NO adsorption, followed by the dissociation of adsorbed NO to N and O species.[14] The activity and selectivity of Pt were found to depend on the used support material[12] and reaction conditions.[15] Particularly at high CO/NO ratios, the deactivation of the Pt-based catalysts with time was shown to take place. By using *in situ* IR spectroscopy, the role of NCO and further surface species in the catalyst deactivation was investigated in more detail but has not been fully clarified so far.[16,17] In contrast, less work has been conducted for more realistic conditions, where O_2 is present in the reaction mixture in addition to CO and NO. In a very recent study, Di et al.[18] reported that NO shifts the onset of CO oxidation toward higher temperatures for Pt/Al_2O_3 and Pt/CeO_2 under oxygen-

Received: March 24, 2025
Revised: June 27, 2025
Accepted: July 2, 2025

rich (fuel-lean) reaction conditions. Based on *in situ* diffuse reflectance infrared Fourier transform spectroscopy (DRIFTS) results, the addition of NO was furthermore assumed to hinder the Mars-van Krevelen pathway for Pt/CeO_2 due to the formation of nitrates on the CeO_2 support.[18] However, the role of NO under stoichiometric and oxygen-poor (fuel-rich) reaction conditions, where reduction phenomena are expected to be more pronounced, is still unclear. Moreover, the structural dynamics of Pt during the catalyst operation has been only partially addressed.

As shown for Pd- and Rh-based catalysts,[19,20] the variation in gas composition and temperature leads to pronounced changes in the chemical state and morphology of the noble metals, thus strongly affecting the catalytic performance during CO and NO conversion. For uncovering and understanding such reaction-induced dynamics, *operando* spectroscopy, including but not limited to complementary X-ray and infrared-based characterization techniques, is an unavoidable tool.[21−23] Additionally, advanced photon-in/-out techniques like high-energy-resolution fluorescence detected X-ray absorption near-edge structure (HERFD-XANES) spectroscopy allow a higher sensitivity than conventional X-ray absorption spectroscopy (XAS).[24,25] Due to conversion and thus a continuously changing gas environment along the catalyst bed, the catalyst state has been shown to vary in the axial position.[26−28] Therefore, not only *operando* investigations but also spatially resolved studies are crucial for deriving structure−performance correlations.

In this work, we aimed at uncovering the impact of NO on the noble metal state and the CO oxidation activity of Pt-based catalysts under close-to-stoichiometric reaction conditions by using spatially resolved *operando* XAS in combination with complementary *in situ*/*operando* characterization techniques. Hereby, the impact of the used support material (CeO_2, Al_2O_3) and the reductive pretreatment on the structural evolution is carefully evaluated for different axial positions by extended X-ray absorption fine structure (EXAFS) and *operando* XANES spectroscopy. Furthermore, we investigated and quantified the contribution of NO adsorbed on the Pt surface during the combined $CO + O_2 + NO$ reaction by *in situ* DRIFTS and more advanced *operando* HERFD-XANES experiments. Such a complementary spectroscopic approach allowed us to follow the formation and evolution of active Pt clusters/particles along the catalyst bed, thus providing more insights into the structural dynamics of Pt during the catalyst operation.

EXPERIMENTAL SECTION

Catalyst Synthesis. Prior to the synthesis, commercial CeO_2 and Al_2O_3 (Puralox, SASOL) supports were calcined in static air at 700 °C for 5 h. For the 1.0 wt % Pt/Al_2O_3 catalyst, the Al_2O_3 support (pore volume of 0.5 mL/g) was loaded in one step with the corresponding amount of the tetraammineplatinum(II) nitrate (STEM Chemicals, 99%) solution by incipient wetness impregnation. Analogous to previous studies,[29,30] the obtained powder was dried at 70 °C for 1 h and calcined at 500 °C for 5 h. The synthesis of 1.0 wt % Pt/CeO_2 was conducted using a robot-controlled synthesis unit (Accelerator SLT106, ChemSpeed Technologies), similar to refs 31 and 32. In each of the reactors, 0.25 mL of tetraammineplatinum(II) nitrate (STEM Chemicals, 99%) solution (200 mg in 9.8 g of H_2O) was added to 0.99 g of CeO_2 (pore volume of 0.25 mL/g). Afterward, the impregnated powder was dried under reduced pressures (below 100 mbar) at 70 °C. To improve the distribution of the noble metal on the CeO_2 support, a diluted noble metal solution was used. This impregnation procedure was repeated 4 times. Finally, the dried powder was calcined at 500 °C for 5 h. To obtain a highly dispersed noble metal catalyst, the calcined Pt/CeO_2 sample was hydrothermally treated in a mixture of 10% H_2O in air at 800 °C for 15 h. The water dosage was stopped during cooling at around 200 °C to prevent water condensation at lower temperatures.

For the HERFD-XANES measurements, a Pt/Al_2O_3 catalyst with a slightly higher noble metal loading of approximately 1.9 wt % and an average Pt particle size of 2 nm was synthesized in a comparable manner using the robot-controlled synthesis unit (Accelerator SLT106, ChemSpeed Technologies) described above, and afterward calcined at 500 °C for 5 h.

***Ex Situ* Characterization.** The elemental composition of the samples was determined by inductively coupled plasma optical emission spectroscopy (ICP-OES) using an iCAP 7600 DUO instrument (Thermo Fisher Scientific). Prior to the elemental analysis, the samples were digested using acids and a pressure digestion system DAB-2. The measurements were repeated three times.

For estimation of the specific surface area and pore volume of the pure supports and noble metal-containing catalysts, the nitrogen physisorption method was used. The physisorption measurements were performed on a BELSORP-mini II instrument (BEL, Inc.). For each measurement, around 100 mg of the sample was used. Prior to the physisorption measurement, the catalyst surface was cleaned under reduced pressure at 300 °C for 2 h. The specific surface area was calculated according to the Brunauer−Emmett−Teller (BET) method.[33]

To obtain information about the crystalline phases present in the synthesized catalyst, powder X-ray diffraction (XRD) measurements were performed using a Bruker Advance D8 diffractometer with nickel-filtered Cu $K\alpha_1$ radiation (wavelength = 0.154 nm). The patterns were recorded in the 2θ range between 10 and 120° with a step size of 0.016° and an acquisition time of 3 s per point.

High-angle annular dark-field scanning transmission electron microscopy (HAADF-STEM) images and energy-dispersive X-ray spectroscopy (EDXS) mappings were acquired with an FEI Themis Z or FEI Themis 300 electron microscope operated at 300 keV to get insights into the distribution of the noble metal entities on the support. The samples were deposited in a dry state on a carbon-supported copper grid. Prior to the sample deposition, the transmission electron microscopy (TEM) grids were plasma cleaned 2 times for 30 s at 50% device power (1070 NanoClean, Fischione Instruments). For the evaluation of the Pt particle size distribution in Pt/Al_2O_3, more than 300 Pt nanoparticles were counted by assuming an ellipsoidal shape.

Catalytic Tests and *Operando* X-ray Absorption Spectroscopy Experiments. For catalytic activity tests, a microcapillary reactor, described in more detail in refs 34 and 35, was used. Similarly to earlier studies,[34−36] the sieved catalyst (100−200 μm sieve fraction) was placed in a quartz capillary and heated by a hot air blower (FMB Oxford). For the study of Pt/CeO_2, 15 mg of the catalyst was loaded in a capillary with an outer diameter of 1.0 mm (wall thickness 0.01 mm). The gas flow was set to 75 mL/min, resulting in a weight hourly space velocity (WHSV) of 30 000 L/($g_{noble\ metal}$ h). To

https://doi.org/10.1021/acs.jpcc.5c01963
J. Phys. Chem. C XXXX, XXX, XXX−XXX

obtain a similar catalyst bed length of approximately 6 mm, 10 mg of Pt/Al_2O_3 was placed in a quartz capillary with an outer diameter of 1.5 mm and a wall thickness of 0.01 mm. The total gas flow was adjusted to 50 mL/min *via* mass flow controllers (Bronkhorst) to maintain a WHSV of 30 000 L/($g_{noble\ metal}$ h). In both cases, a few mg of quartz powder were placed at the beginning and end of the catalyst bed to obtain a defined initial and final position. During the catalytic tests, the samples were heated stepwise to 500 °C (step sizes of 50−100 °C) before cooling to room temperature. The catalytic activity of Pt/Al_2O_3 and Pt/CeO_2 was evaluated under close-to-stoichiometric reaction conditions (slightly rich, $\lambda < 1$). These conditions are typical for the simultaneous CO and NO removal over noble-metal-based catalysts.[37] On the other hand, in a slightly reductive gas atmosphere, a fast decrease in activity due to Pt cluster/particle redispersion on CeO_2 is prevented.[30] The following conditions were investigated:

(a) CO oxidation (1.0% CO, 0.5% O_2 in He) using as-prepared catalysts,
(b) CO/NO reaction (1.0% CO, 1000 ppm NO, 0.45% O_2 in He) using as-prepared catalysts,
(c) CO/NO reaction (1.0% CO, 1000 ppm NO, 0.45% O_2 in He) using prereduced catalysts.

The reductive pretreatment for experiment (c) was conducted in 1.0% CO in He at 400 °C for 1 h. The gas concentration was determined at the reactor outlet using an online mass spectrometer (Omnistar GSD 320, Pfeiffer Vacuum) and a Fourier transform infrared spectrometer (Multigas 2030 FTIR Continuous Gas Analyzer, MKS Instruments). The CO and NO_x conversion values were calculated from the gas concentration measured at the reactor outlet. Since a few parts per million of NO_2 were present in the reaction mixture during the experiments, NO_x was defined as the sum of NO and NO_2.

During these catalytic tests, *operando* XAS data were collected at the Pt L3 edge. The *operando* XAS measurements were conducted at the P65 beamline of the synchrotron radiation facility DESY, Hamburg, Germany. Monochromatization of the incident X-ray beam was performed using Si(111) DCM. The beam size was set to 0.3 mm in height and 1.0 mm in width. For both catalysts, XAS measurements were performed in a spatially resolved manner at each temperature step in fluorescence mode using a 4 pixel SDD fluorescence detector (Hitachi/Vortex). Hereby, 5 positions along the catalyst bed were selected. The selected positions were labeled as positions 1 to 5 starting from the beginning (pos. 1) to the end (pos. 5) of the catalyst bed. Before and after the catalytic cycle, EXAFS spectra were recorded along the catalyst bed at room temperature. At each position (positions 1−5), three EXAFS spectra (energy range of 11 418−12 566 eV) were recorded and merged for further analysis. After background subtraction and Fourier transformation in a k range of 3−10 $Å^{-1}$, the EXAFS fitting was performed in an R-space of 1.1−3.3 Å using a multiple k weighting (k_w) = 1, 2, 3. For the EXAFS analysis, the Artemis program from the IFFEFIT software package[38] was used. A combination of bulk PtO_2 (ICSD 4415) and metallic Pt (ICSD 243678) models was used to mimic the experimental spectra. Further details on the EXAFS fitting procedure are provided in the Supporting Information (SI).

The linear combination analysis (LCA) of the XANES spectra (energy range of 11 418−11 991 eV) recorded at different temperature steps was performed in the energy range from 11 544 to 11 594 eV with the following references for 1.0% Pt/Al_2O_3: (1) Pt-ox: 1.0% PtO_2 in cellulose inside a Kapton capillary. (2) Pt-red: Prereduced 1.0% Pt/Al_2O_3 at 500 °C in 1.0% CO, 1000 ppm NO, 0.45% O_2 in He. (3) Pt-CO: Prereduced 1.0% Pt/Al_2O_3 still in 1.0% CO in He at 50 °C. For 1.0% Pt/CeO_2, the following references were selected: (1) Pt-ox: 1.0% PtO_2 in cellulose inside a Kapton capillary. (2) Pt-red: Prereduced 1.0% Pt/CeO_2 at 500 °C in 1.0% CO, 1000 ppm NO, 0.45% O_2 in He. Data treatment (calibration, alignment, normalization) was performed using the Athena program from the IFFEFIT software package,[38] while the LCA was conducted with the Fastosh software (version 1.0.7).[39] For the 1.0% Pt/CeO_2 catalyst, no energy alignment of the XANES spectra was possible, as the CeO_2 support strongly absorbs the X-rays. Due to a high similarity between the XANES spectra of Pt-red and Pt-CO (see the SI) in combination with the missing energy alignment, only Pt-ox and Pt-red were used as LCA references for Pt/CeO_2 to ensure robustness of the fits.

***Operando* High-Energy-Resolution Fluorescence Detected X-ray Absorption Near-Edge Structure.** HERFD-XANES measurements were conducted at the ID26 beamline at ESRF.[40] Three 1.6 m undulators (3.5 cm period) were used for X-ray generation, and three Pd-coated mirrors were utilized for the removal of harmonics. A Si(311) double-crystal monochromator was used to tune the energy of the incident beam (Pt L3 edge). The photon flux at the sample at ID26 was below $2 \times 10^{12} \frac{1}{s}$ with a bandwidth of 0.3×10^{-4}. Five Ge(660) spherical bent analyzers on a Rowland circle were utilized for the selection of the $L_{\alpha 1}$ emission line. The beam size used for the experiments was set to 100 (h) × 200 (w) μm^2. During the experiments, a 1.9 wt % Pt/Al_2O_3 catalyst was used. Similarly to *operando* XAS measurements described above, the sieved catalyst powder (100−200 μm) was placed inside a quartz reactor with an outer diameter of 1.5 mm and 0.02 mm wall thickness (WJM-Glas, Müller GmbH) and heated by a hot air blower (FMB Oxford). Gasses were dosed by mass flow controllers (Bronkhorst) with a WHSV of 25 000 L/($g_{noble\ metal}$ h). Prior to the experiments, the average temperature within the region of interest where HERFD-XANES spectra were recorded was determined by IR thermography in relation to the temperature set point (ImageIR 8300 camera, InfraTec). Analogous to the *operando* XAS experiments, the gas conversions were calculated based on the FTIR (Multigas 2030 FTIR Continuous Gas Analyzer, MKS Instruments) data recorded at the reactor outlet. The NO_x concentration was defined as the sum of the NO and NO_2. However, since no NO_2 was detected during the reaction, only the NO concentration was used for the calculation of the NO_x conversion. Prior to the experiments, the catalyst was prereduced. Hereby, a gas mixture of 2% H_2 in He was applied while the catalyst was heated with 7 °C/min to 500 °C. After 10 min at 500 °C, the sample was cooled to room temperature, where the gas mixture was changed and the respective experiment was conducted. Data analysis was performed using the Fastosh software[39] (version 1.0.7). For data normalization, the following parameters were applied with respect to E_0: Pre-edge normalization from −16 to −12 eV; post-edge normalization from 29 to 42 eV with a polynomial function degree of 0. In the case of the Pt-ox reference, the post-edge normalization parameters were slightly adjusted to ensure a consistent normalization at high energies (from 20 to 45 eV with a polynomial function degree of 1).

https://doi.org/10.1021/acs.jpcc.5c01963
J. Phys. Chem. C XXXX, XXX, XXX−XXX

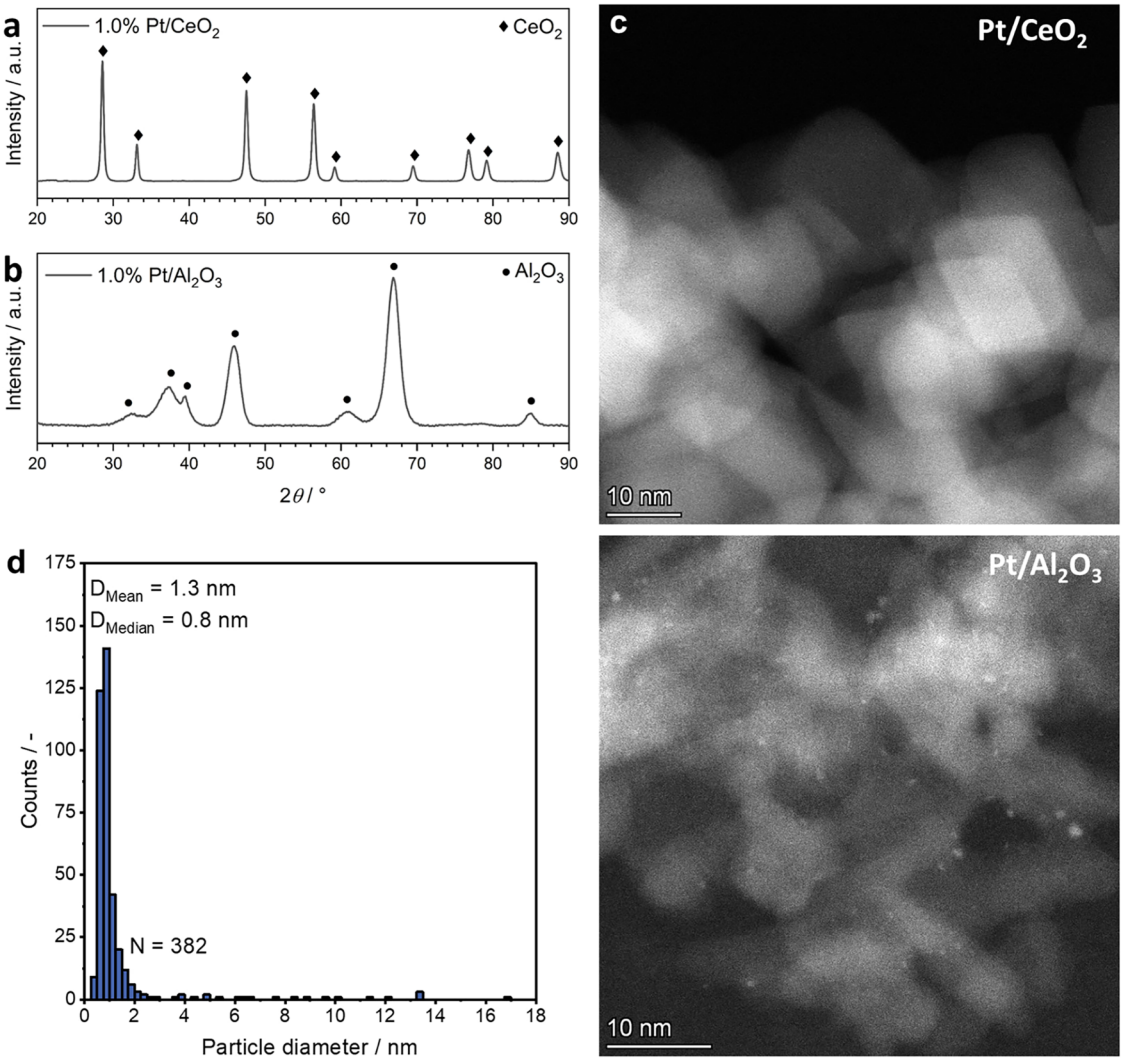

Figure 1. XRD patterns (a, b) and HAADF-STEM images of 1.0% Pt/CeO_2 (c) and 1.0% Pt/Al_2O_3 with corresponding particle size distribution (d). The assignment of the XRD reflections was performed based on the data from the crystallographic database (ICSD CeO_2: 24887, ICSD Al_2O_3: 249140).

For the reference spectra used for the LCA, the Pt/Al_2O_3 catalyst was heated to 500 °C in 2% H_2/He. After a holding time of 10 min, the sample was cooled to room temperature in 2% H_2/He. The recorded HERFD-XANES spectrum corresponded to the metallic "Pt" reference. Afterward, the gas mixture was switched to 0.2% NO/He to obtain the "Pt-NO" reference spectrum. For the "Pt-ox" and "Pt-CO" references, a new Pt/Al_2O_3 sample was used. This sample was exposed to a gas flow of 0.5% O_2/He at room temperature, where the "Pt-ox" reference spectrum was recorded. Afterward, the sample was heated in 2% H_2/He to 500 °C and cooled to room temperature after 10 min at 500 °C. At room temperature, the sample was exposed to 0.1% CO/He to obtain the "Pt-CO" reference spectrum. For the collection of all reference spectra, the WHSV of 25 000 L/($g_{noble\ metal}$ h) was applied. To verify that the "Pt-ox" reference spectrum represented a fully oxidized catalyst, another Pt/Al_2O_3 sample was calcined for 10 min in static air at 500 °C. This sample was afterward measured in static air at room temperature and revealed an HERFD-XANES spectrum identical to that of Pt-ox, described above.

***In Situ* Diffuse Reflectance Infrared Fourier Transform Spectroscopy.** Diffuse reflectance infrared Fourier transform spectroscopy (DRIFTS) measurements were performed on a VERTEX 70 Fourier transform infrared spectrometer (Bruker) equipped with Praying Mantis diffuse reflection optics (Harrick) and a liquid nitrogen-cooled mercury cadmium telluride detector. The catalysts were diluted with CaF_2 (Thermo Scientific, 99.5%) in a ratio of 1:4, sieved (sieve fraction 100−200 μm) and placed in a high-temperature *in situ* cell (Harrick) covered with a CaF_2 window. Similar to a previous study,[41] a correlation between the temperature of the catalyst surface and the set point was estimated with an ImageIR 8300 camera (InfraTec). The temperature values given in this work are based on the temperatures obtained with the IR camera, which provides only the surface temperature of the catalyst bed. To determine the surface adsorbates as a function of the reaction mixture and evaluate the effect of NO on the catalyst state, adsorption experiments (total gas flow of 100 mL/min) were performed for the Pt/Al_2O_3 and Pt/CeO_2 catalysts. Without changing the samples, gas adsorption experiments were conducted in the following order, with each step lasting 1 h: (1) 1000 ppm NO/Ar; (2) 1000 ppm NO + 1000 ppm CO/Ar; (3) 1000 ppm NO + 1.0% CO/Ar; (4) 1000 ppm NO + 1.0% CO + 0.45% O_2/Ar; (5) 1.0% CO/

https://doi.org/10.1021/acs.jpcc.5c01963
J. Phys. Chem. C XXXX, XXX, XXX−XXX

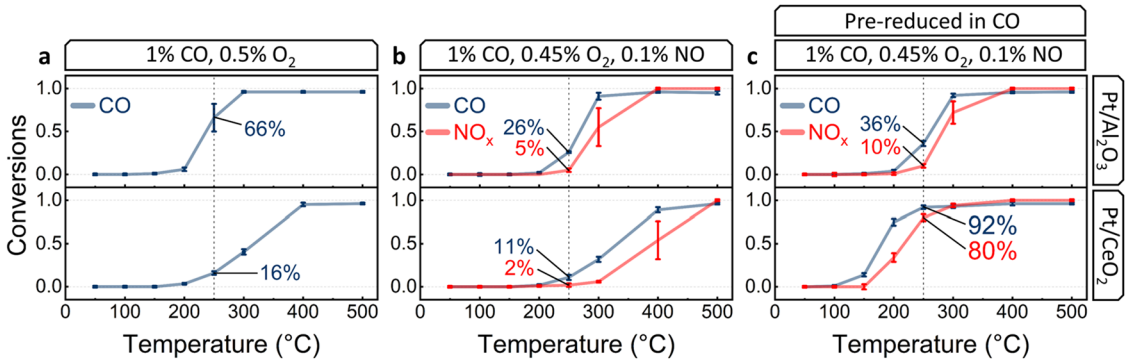

Figure 2. CO and NO conversions for 1.0% Pt/Al_2O_3 (top) and 1.0% Pt/CeO_2 (bottom) during the CO + O_2 (a) and the CO + O_2 + NO reaction under slightly rich conditions without (b) and with (c) a prereduction step (WHSV = 30 000 L/($g_{noble\ metal}$ h)). In order to compare the conversions for different catalysts and gas mixtures, the CO and NO conversions at 250 °C are depicted as insets. The error bars represent the activity variation during each measurement.

Ar. The spectrum recorded at room temperature after the catalyst pretreatment (1 h at 350 °C in 10% O_2/Ar, 100 mL/min) was used as background spectrum for all adsorption experiments. The recorded DRIFTS data (4 cm^{-1} resolution; 100 spectra) were converted into absorbance by using the OPUS software (Bruker).

RESULTS AND DISCUSSION

Initial Catalyst State. The structures of the Pt/CeO_2 and Pt/Al_2O_3 catalysts and the Pt particle size were determined *ex situ* using HAADF-STEM and XRD characterization data. As can be seen in Figure 1a,b, the XRD patterns of both catalysts show only reflections corresponding to the support materials, indicating the presence of small Pt nanoparticles below 2 nm and/or amorphous noble metal phases. According to the HAADF-STEM images in Figure 1c, no Pt particles could be detected in the 1.0% Pt/CeO_2 catalyst confirming a high Pt dispersion as single atoms/clusters over the entire support after the hydrothermal treatment at 800 °C, in agreement with existing literature.[31,42,43] In contrast, Pt nanoparticles with an average diameter of 1.3 nm (mean diameter of 0.8 nm) were observed in 1.0% Pt/Al_2O_3 (Figure 1d).

Impact of Reaction Conditions on the Final Catalyst State. To investigate the influence of NO on the activity and structural evolution of the selected Pt-based catalysts, the CO oxidation reaction under close-to-stoichiometric conditions (slightly rich, $\lambda \lesssim 0.99$) was conducted in the presence/absence of NO. Since Pt/CeO_2 and Pt/Al_2O_3 exhibited different initial states (Figure 1), a reductive pretreatment was additionally applied prior to the combined CO + O_2 + NO reaction to initiate the formation of Pt particles. The obtained catalytic activity results are listed in Figure 2.

Without the prereduction step, the catalytic performance data obtained for the Pt-based samples display the onset of CO conversion at around 200 °C, while NO was converted above 300 °C during the combined reaction (Figure 2a,b). After the reductive treatment, the light-off profiles were shifted to lower temperatures for both samples (Figure 2c). In the following, the different catalytic activities observed at 250 °C (partial CO and NO conversion over all samples) are compared in more detail. As can be seen from Figure 2a, the Al_2O_3-supported Pt catalyst showed a better CO oxidation activity in the as-prepared state in comparison to Pt/CeO_2 (X_{CO} = 66 vs 16% under NO-free conditions). In the presence of NO (Figure 2b), a lower CO conversion was reached at 250 °C for both Pt-based samples (X_{CO} = 26% for Pt/Al_2O_3 vs 11% for Pt/CeO_2). In the literature, such an activity decrease is often attributed to competitive adsorption of CO and NO.[44] The reductive treatment positively influenced the CO/NO_x conversion independent of the support material (Figure 2c) but had a stronger effect on the 1.0% Pt/CeO_2 sample. In this case, the CO and NO_x conversion values at 250 °C increased from 11 to 92% for CO and from 2 to 80% for NO_x. On the contrary, only a moderate increase in activity was observed for Pt/Al_2O_3 (X_{CO} = 36%; X_{NO_x} = 10%). The stronger influence of the reductive treatment on Pt/CeO_2 can be explained by a more significant structural change in this case during the reduction. While Pt was highly dispersed in the hydrothermally treated CeO_2-supported catalyst, the 1.0% Pt/Al_2O_3 sample contains larger Pt clusters and particles already in the as-prepared state (Figure 1). Prereduction treatments are known to promote the formation of active Pt clusters in Pt/CeO_2,[30,31,45,46] leading to the activity boost during CO oxidation. Furthermore, the increase in catalytic performance can also be attributed to the activation of the Pt/CeO_2 interface that is crucial for a high CO oxidation activity at low temperatures.[47]

The observed catalytic trends also clearly illustrate that, independent of the support and catalyst pretreatment, the conversion of NO always takes place at higher temperatures than the conversion of CO. This behavior confirms that CO reacts at first with O_2 and only tends to react with NO at higher temperatures. As reported in the literature for Pt/Al_2O_3 catalysts, the NO dissociation represents the rate-determining step in the CO + NO reaction.[13,48−50] Therefore, it can be assumed that the lack of empty Pt sites inhibits NO dissociation and the onset of the CO + NO reaction at low temperatures. This effect can be overcome at higher CO conversion values, where the number of empty Pt sites available for NO dissociation increases. The similar trend observed for the 1.0% Pt/Al_2O_3 and 1.0% Pt/CeO_2 samples can be further explained by a stronger contribution of the Langmuir−Hinshelwood pathway to the overall reaction at higher temperatures[47] while the Mars-van Krevelen Mechanism contributes substantially at low temperatures for Pt/CeO_2.[47,51]

In order to reveal the impact of reaction conditions on the structure of Pt in the catalysts, EXAFS spectra were recorded before and after the above-mentioned catalytic tests at room temperature. For the EXAFS analysis, a combination of two structural models, namely, bulk PtO_2 and metallic bulk Pt, was

https://doi.org/10.1021/acs.jpcc.5c01963
J. Phys. Chem. C XXXX, XXX, XXX−XXX

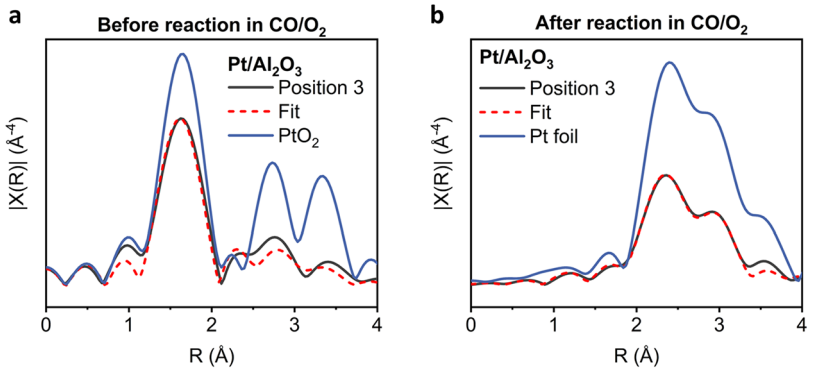

Figure 3. Fourier transform EXAFS spectra (Pt L3 edge, k^3-weighted) recorded at the middle position (pos. 3) of the 1.0% Pt/Al_2O_3 catalyst bed before (a) and after (b) the CO + O_2 reaction (1.0% CO/0.5% O_2/He, WHSV = 30 000 L/($g_{noble\ metal}$ h)) with the corresponding fits as well as PtO_2 (a) and metallic Pt (b) references.

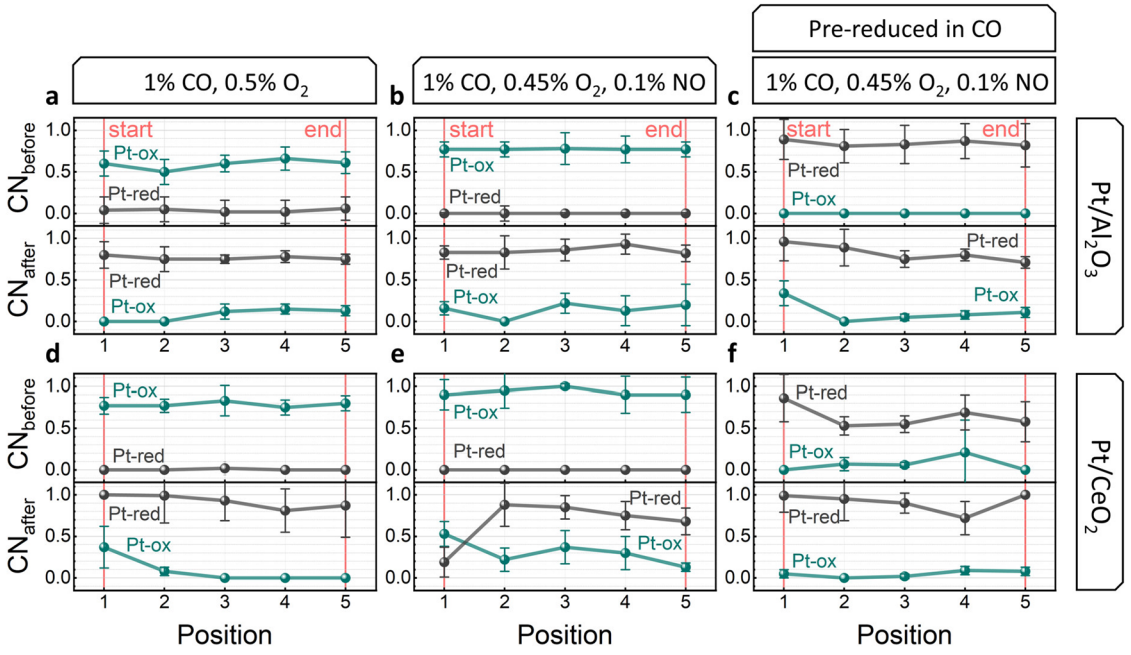

Figure 4. Relative coordination number (CN) based on the bulk PtO_2 (Pt-ox) and metallic bulk Pt (Pt-red) contributions from the EXAFS analysis of 1.0% Pt/Al_2O_3 (a–c) and 1.0% Pt/CeO_2 (d–f) for the CO + O_2 and the CO + O_2 + NO reactions under slightly rich conditions with and without a prereduction step. Each experimental data set was recorded in the corresponding reaction mixture at room temperature, before (top) and after (bottom) reaction. EXAFS spectra of the prereduced catalysts before reaction were collected in 1.0% CO/He. Positions 1 to 5 represent equally distributed positions from the beginning (pos. 1) to end (pos. 5) of the catalyst bed.

used. In the combined fitting model, the single scattering paths representing the Pt–O (R_{eff} = 1.975 and 2.020 Å) and Pt–O–Pt (R_{eff} = 3.138 Å) contributions in bulk PtO_2 were included together with the single scattering Pt–Pt path (R_{eff} = 2.774 Å) in bulk Pt. To illustrate the structural change under reaction conditions, the Fourier transform EXAFS spectra obtained for the 1.0% Pt/Al_2O_3 catalyst at the middle position (pos. 3) of the catalyst bed before and after the CO oxidation reaction are reported in Figure 3 together with the corresponding EXAFS fitting results (further details on the EXAFS analysis are provided in the SI.)

To facilitate the comparison between the samples, relative coordination numbers (CNs) of bulk PtO_2 and bulk Pt divided by the degeneracy of the paths are given in Figure 4 for all investigated reaction conditions. These relative coordination numbers help to visualize the contribution of the bulk PtO_2 (Pt-ox) and bulk Pt (Pt-red) models to the overall fit. The catalysts were probed at different axial positions in the microreactor, with positions 1 and 5 representing the beginning and end of the catalyst-packed powder bed, respectively.

As can be seen in Figure 4a,d for the CO + O_2 reaction, the noble metal in both catalysts was in an oxidized state prior to the light-off, and no contribution of metallic bulk Pt was obtained during EXAFS fitting. The coordination number of Pt-ox contribution along the catalyst bed was lower for the Pt/Al_2O_3 catalyst ($CN_{average}$(Pt-ox) ≈ 0.6) than for Pt/CeO_2 ($CN_{average}$(Pt-ox) ≈ 0.8). The higher initial coordination number of Pt-ox for the CeO_2 support (Figure 4d vs Figure 4a) can be explained by the presence of highly dispersed, oxidized Pt species in the as-prepared Pt/CeO_2 catalyst in comparison to the particle-containing Pt/Al_2O_3 catalyst (Figure 1). After the CO oxidation reaction, a strong reduction of Pt was observed particularly at mid- and end positions in the

https://doi.org/10.1021/acs.jpcc.5c01963
J. Phys. Chem. C XXXX, XXX, XXX–XXX

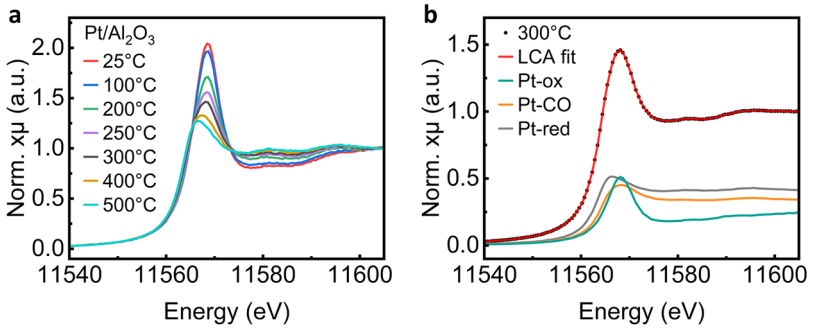

Figure 5. Normalized XANES spectra (Pt L3 edge) recorded at the middle position (pos. 3) of the 1.0% Pt/Al_2O_3 catalyst bed during the CO + O_2 reaction (1.0% CO/0.5% O_2/He, WHSV = 30 000 L/($g_{noble\ metal}$ h)) (a) and the selected LCA result together with the contribution of the LCA references for the XANES measurement at 300 °C (b).

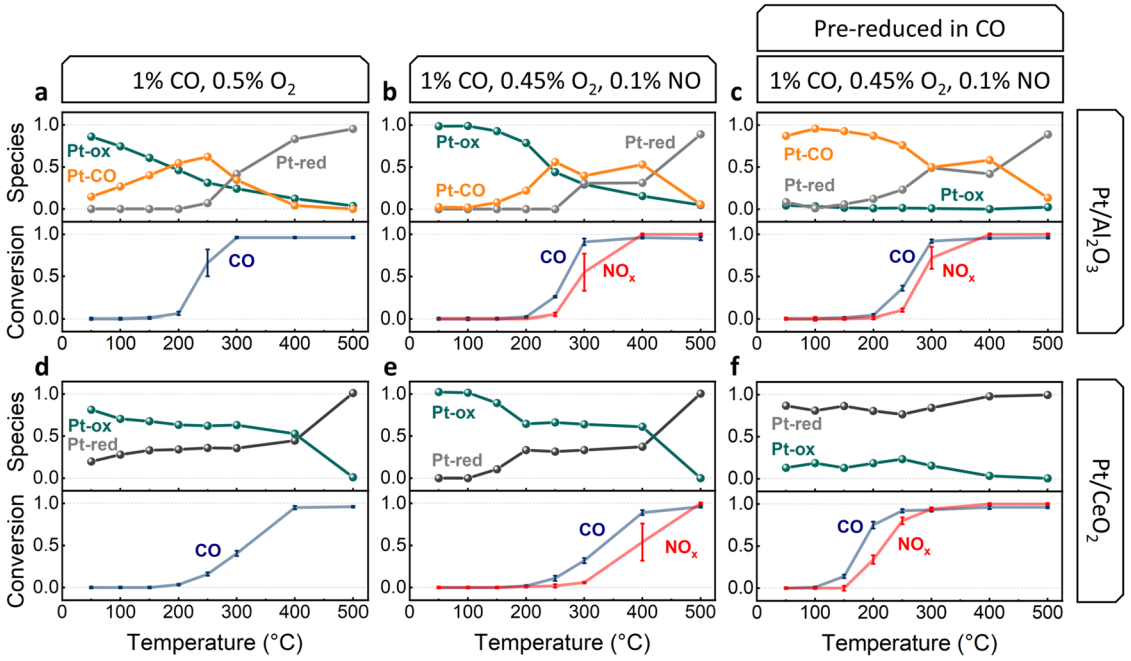

Figure 6. Catalytic activity in terms of gas conversion and evolution of Pt species in 1.0% Pt/Al_2O_3 (a–c) and 1.0% Pt/CeO_2 (d–f) during the CO + O_2 and the CO + O_2 + NO reaction under slightly rich conditions with and without a prereduction step (WHSV = 30 000 L/($g_{noble\ metal}$ h)). The XANES spectra were recorded in the middle of the catalyst beds (pos. 3). Pt species: Pt-ox = fraction of oxidized Pt; Pt-red = fraction of reduced Pt; Pt-CO = fraction of CO covered, reduced Pt.

catalyst bed, which is indicated by a prominent increase in the normalized coordination number of metallic bulk Pt with an average coordination number of 0.8 for Pt/Al_2O_3 (Figure 4a) and 0.9 for Pt/CeO_2 (Figure 4d). These changes can be linked to the slightly rich conditions and the excess of CO during the reaction, which caused Pt reduction and the formation of nanoparticles. In comparison to the other positions, a higher contribution of Pt-ox was observed at the inlet position (pos. 1) for Pt/CeO_2 after the CO oxidation reaction (Figure 4d, bottom), which indicates a slightly more oxidized state at the beginning of the catalyst bed. The formation of a gradient in Pt local structure can be explained by the reaction occurring mostly at the reactor inlet at elevated temperatures, as previously reported for noble-metal-based systems during CO oxidation.[36,52] Since the catalytic tests in this study were conducted under slightly rich conditions, the catalyst outlet was exposed to lower oxygen concentrations at high temperatures and was more reduced during the reaction. On the contrary, the presence of O_2 in the gas phase at the inlet position can lead to a decrease in the rate of Pt particle formation, and even favors Pt reoxidation/redispersion to a minor extent.[30]

Figure 4b,e displays the results of the EXAFS evaluation for the combined CO + O_2 + NO gas mixture. With the replacement of 500 ppm O_2 by 1000 ppm NO, Pt showed a higher initial oxidation state over both support materials. Compared with the CO + O_2 feed, the coordination number of Pt-ox contribution increased from 0.6 to 0.8 for Pt/Al_2O_3 (Figure 4a,b) and from 0.8 to 0.9 for Pt/CeO_2 (Figure 4d,e). These findings underline an oxidative effect of NO on Pt for both samples or adsorption on the noble metal surface, preventing its reduction by CO. A significant increase in Pt oxidation state was also reported by Gänzler et al. for a Pt/Al_2O_3 catalyst during lean CO/NO oxidation.[53] Analogous to the trends observed in the CO + O_2 gas mixture, a strong reduction of Pt was revealed after the reaction by EXAFS data analysis. For the 1.0% Pt/Al_2O_3 catalyst (Figure 4b), a similar noble metal state was obtained along the entire catalyst bed

https://doi.org/10.1021/acs.jpcc.5c01963
J. Phys. Chem. C XXXX, XXX, XXX−XXX

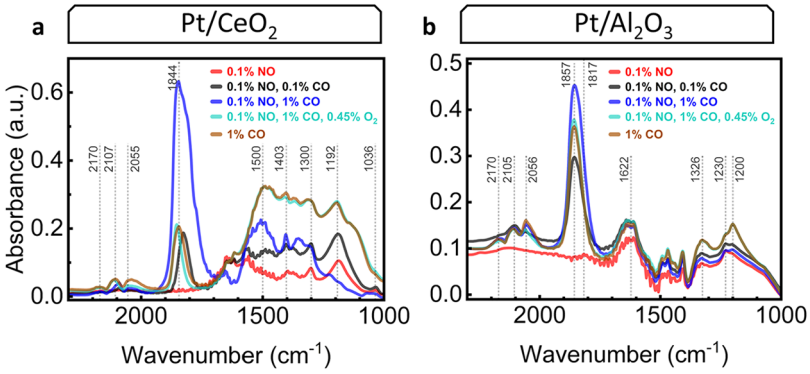

Figure 7. DRIFT spectra recorded at 30 °C in different CO/NO-containing mixtures for 1.0% Pt/CeO_2 (a) and 1.0% Pt/Al_2O_3 (b). Each gas mixture was dosed for 60 min in the given order (from top to bottom) before changing the composition.

($CN_{average}$(Pt-red) ≈ 0.8). In this case, the fractions of Pt-red and Pt-ox were comparable to those observed after the CO + O_2 reaction (Figure 4a). In contrast, for Pt/CeO_2, a different behavior was detected, with the beginning of the catalyst bed significantly more oxidized compared with the other downstream positions (positions 2−5). To be noted is the considerably lower fraction of Pt−Pt backscattering (CN(Pt-red) ≈ 0.2) at position 1. Furthermore, the structural gradient observed at the inlet positions of the catalyst bed was more pronounced compared with the CO-only oxidation conditions (Figure 4d,e). Thus, these observations demonstrate a clear influence of NO on the catalyst evolution under reaction conditions, in particular a lower degree of Pt reduction and particle formation at the beginning of the catalyst bed. This evolution can also be linked to a later onset of the CO oxidation reaction in the presence of NO, leading to the less reducing condition upstream at higher temperatures.

After the reductive treatment in 1.0% CO at 400 °C for 1 h, Pt was in an almost fully reduced state in both catalysts before the reaction (Figure 4c,f), as confirmed by the considerable contribution of metallic bulk Pt ($CN_{average}$(Pt-red) = 0.85 for Pt/Al_2O_3 and 0.6 for Pt/CeO_2). For the 1.0% Pt/Al_2O_3 system (Figure 4c), the overall coordination numbers of Pt observed after reaction remained similar to those of the prereduced catalyst. However, it should be noted that the presence of large noble metal nanoparticles (above 3 nm)[54] cannot be excluded by means of EXAFS due to the lower sensitivity of this method for larger particles. In contrast, a more pronounced reduction was observed for the 1.0% Pt/CeO_2 catalyst, as indicated by the increased metallic Pt contribution after the reaction (Figure 4f). Such a behavior can be explained by the slightly rich reaction conditions and the earlier ignition of CO oxidation and NO reduction, providing more time for the Pt atoms to reduce and form larger nanoparticles, in contrast to the Pt/Al_2O_3 catalyst. As a consequence of the longer reduction, no pronounced structural gradients were observed for Pt/CeO_2.

Thus, the conducted EXAFS measurements confirm the expected strong reduction of both catalysts under slightly rich conditions. For the 1.0% Pt/CeO_2 catalyst, this reduction also goes along with the Pt particle formation. To obtain deeper insights into the transient behavior of Pt under the reaction conditions and reveal the origin of the diminished CO oxidation activity, *operando* XANES measurements were performed at different temperatures.

Structural Evolution of Pt Followed by *Operando* XAS. *Operando* XANES spectra were recorded at different reaction temperatures (25−500 °C) and axial positions and subsequently evaluated by linear combination analysis (LCA), as selectively shown for Pt/Al_2O_3 during CO oxidation in Figure 5. The LCA results, illustrating the evolution of the Pt chemical state at the middle position of the catalyst bed (pos 3), are depicted for the investigated samples together with the catalytic activity in Figure 6. The trends in catalytic performance were already discussed in the previous section (see Figure 2), and are additionally shown here for deriving structure−activity correlations.

The initial chemical state of the noble metal in Pt/Al_2O_3 (Figure 6a) in a CO + O_2 atmosphere was almost fully oxidized (Pt-ox = 0.86) with a minor contribution of Pt-CO. With increasing temperature, the surface oxygen is partially replaced by CO, as shown by the higher fraction of Pt-CO. With the ongoing CO conversion, the adsorbed CO reacts with dissociated oxygen to CO_2 according to the Langmuir−Hinshelwood mechanism.[36,55] Above 300 °C, the Pt surface coverage decreased due to desorption processes, leading to the increase in the metallic Pt component (Pt-red). In order to understand the effect of NO on the chemical state of Pt, 500 ppm O_2 in the gas mixture was replaced by 1000 ppm NO. As visualized in Figure 6b, the Pt-CO species are replaced by Pt-ox at low temperatures, which indicates that NO had an oxidizing effect on Pt. This effect was also observed in the case of the Pt/CeO_2 catalyst at low temperatures (Figure 6d,e). Furthermore, the replacement of Pt-CO (reduced Pt for Pt/CeO_2) by Pt-ox may indicate the competitive adsorption of CO and NO on the Pt surface.

After the reductive pretreatment (Figure 6c,f), both catalysts were present in a reduced chemical state. In contrast to Pt/Al_2O_3, the Pt/CeO_2 catalyst still exhibited a minor contribution of Pt-ox (≈0.13) after the prereduction step. This fact can be explained by the strong interaction between Pt and CeO_2, involving oxygen transfer from CeO_2 to Pt and electron transfer from Pt to the support material.[56] Such an electron transfer from Pt to CeO_2 was found to be the largest for Pt particles containing approximately 50 atoms[57] leading to the formation of partially oxidized Pt. Furthermore, the involvement of the Pt-CeO_2 interface in the reaction mechanism at low temperatures (Mars-van Krevelen mechanism)[47] is responsible for the improvement seen in the catalytic activity (Figure 6e vs Figure 6f). Note that this mechanism is known to occur for the redox active CeO_2 support but not for Al_2O_3, which explains a lower enhancement of the catalytic activity and the absence of fraction of Pt-ox for Pt/Al_2O_3. Analogously to the trends described above,

https://doi.org/10.1021/acs.jpcc.5c01963
J. Phys. Chem. C XXXX, XXX, XXX−XXX

further reduction was observed at high conversion values for both catalysts, as shown by the increased fraction of the Pt-red reference.

Even though the references selected for LCA seem to be sufficient to mimic the experimental XANES spectra, the contribution of further adsorbates to the overall fit can not be extracted. To identify and quantify the role of relevant surface species on Pt, *in situ*/*operando* characterization techniques with higher surface sensitivity were applied in the next step.

Identification and Quantification of Surface Species on Pt. During the analysis of the *operando* XAS data, only the presence of the Pt-red, Pt-ox, and Pt-CO species was considered. The existence and contribution of further relevant surface adsorbates, especially during the CO + O_2 + NO reaction, could not be resolved by conventional *operando* XAS due to a limited surface sensitivity, and in the case of single atoms/clusters sufficiently resolved XANES spectra. Therefore, *in situ* DRIFTS measurements were performed for different CO/NO-containing gas mixtures to gain insight into the interaction of individual reactants with Pt and study the adsorbates present on the catalyst surface.

In the DRIFT spectrum of the Pt/CeO_2 catalyst (Figure 7a), IR bands in the region of 1700−1000 cm^{-1} emerged during adsorption of 1000 ppm NO. These bands correspond to NO molecules adsorbed on the support material, forming nitrates and nitrites.[58−61] The absence of IR bands above 1700 cm^{-1} indicates that NO does not strongly adsorb on the highly dispersed, oxidized Pt atoms (Figure 7a, red). With the introduction of 1000 ppm of CO into the gas feed, new adsorption bands appear in the 1700−1100 cm^{-1} region, corresponding to C-containing surface species on the CeO_2 support, e.g., carbonates, carboxylates, or related species.[62−64] Furthermore, additional IR bands of low intensity at 2093 and 2039 cm^{-1} and an intense band at 1828 cm^{-1} were detected during this experiment (Figure 7a, black). The IR band at 2093 cm^{-1} is assigned to CO adsorbed on oxidized Pt clusters, while a shoulder at around 2039 cm^{-1} originates from CO on reduced Pt clusters, which are formed upon CO exposure.[65,66] Since the IR band at 1828 cm^{-1} was not detected during the adsorption experiments with CO only (Figure S25), this band probably corresponds to NO species adsorbed on Pt atoms. In the literature, the IR bands in the range 1820−1840 cm^{-1} have been associated with NO molecularly adsorbed on defect Pt sites.[67] For a higher CO concentration in the gas feed (Figure 7a, blue), a new asymmetric IR band at 1845 cm^{-1} with a shoulder at 1830 cm^{-1} was observed in the DRIFT spectrum. The intensity of this band decreased, and the shoulder vanished after introduction of O_2 (Figure 7a, green). After switching off the O_2 and NO dosage, no intensity increase of the band at 1845 cm^{-1} was observed (as shown in Figure 7a, brown). In the literature, the band at 1845 cm^{-1} is often assigned to bridged CO adsorbed on metallic Pt sites.[68,69] However, no prominent band was detected in this range during the CO adsorption experiments, as observed in this work (Figure S25) and also reported in the literature[70] for similar systems at comparable CO concentration. To investigate the possible influence of the dilution material (CaF_2) on the appearance of the IR bands during our investigations, the NO-only and the combined CO/NO adsorption experiment were additionally conducted with an undiluted Pt/Al_2O_3 sample. The results of these measurements are reported in Figure S28. In general, the dilution of a sample with a nonabsorbing material is applied to minimize the specular reflectance and increase the diffuse reflectance component. However, the type of diluting matrix can affect the position and intensity of the IR bands if an interaction is present with the sample of interest or reactant gases.[71] In this study, similar profiles of the DRIFTS spectra were obtained for the undiluted Pt/Al_2O_3 catalyst in comparison to those obtained for this sample after dilution with CaF_2. The slight shift of the NO-related bands reported in Figure 7b versus the data shown in Figure S28 indicates that at this low temperature (30 °C) only minor catalyst−dilutant−adsorbent interactions are present, which do not influence our assignments significantly. As described by Ivanova et al.,[72] this IR band can also be related to nitrosyl species adsorbed on metallic or positively charged Pt atoms. The DRIFTS data thus indicate competitive adsorption not only between CO and NO but also between O_2 and NO on the Pt surface. Nevertheless, it should be noted that there is no uniform assignment of the IR bands for the NO and CO species existing in the literature. However, it can be concluded that the CO-induced restructuring of the highly dispersed Pt species is crucial for improvement of the CO/NO adsorption ability of the catalyst. To evaluate the influence of the Pt particle size and the CeO_2 support on the evolution of the spectra, the same experiments were conducted with 1.0% Pt/Al_2O_3 (Figure 7b). In contrast to Pt/CeO_2, a band at 1817 cm^{-1} corresponding to Pt-NO species[73] was observed in the DRIFT spectrum of the as-prepared Pt/Al_2O_3 during NO dosage, in addition to those corresponding to NO adsorbed on the support material (Figure 7b, red). As reported by Primet et al.,[74] the position of the Pt-NO-band is strongly dependent on the size of Pt particles and is shifted to lower wavenumbers with increasing Pt particle size, which is in line with the presence of small Pt particles with a size around 1.5 nm in the Pt/Al_2O_3 sample. In contrast to Pt/CeO_2, the IR band at 1857 cm^{-1}, associated with Pt-NO species, was detected already during the first combined CO/NO adsorption measurement (Figure 7b, black), but no shoulder was observed at around 1830 cm^{-1} with increasing the CO pressure in the gas mixture (Figure 7b, blue). The absent IR band at 1830 cm^{-1} might be a possible indication of a lower number of defect sites available in the particles formed in the Pt/Al_2O_3 catalyst. After the addition of O_2 to the gas mixture, the intensity of the IR band at 1857 cm^{-1} slightly decreased (Figure 7b, green), but to a much lower extent compared to Pt/CeO_2 (Figure 7a). No further changes were detected after stopping the NO and O_2 dosage (Figure 7b, brown). The IR bands at 2105 and 2056 cm^{-1}, corresponding to CO adsorbed on partially reduced Pt nanoparticles,[75] were detected during all DRIFTS experiments with CO-containing gas mixtures.

In summary, the DRIFTS results confirm the strong influence of the gas composition on the Pt state. Competitive adsorption between CO and NO was observed for both Pt-based catalysts. However, a quantification of the Pt-NO contribution for different reaction temperatures is very challenging based on only the DRIFTS results. In this regard, HERFD-XANES is a powerful tool for revealing the influence of surface adsorbates on the electronic structure of noble metals.[24,25,47,76−78] Hence, HERFD-XANES measurements were performed to further investigate and quantify the effect of the Pt-NO interaction on the overall reaction over a broad temperature range. Hereby, different CO/NO ratios were used to better estimate the impact of the presence of NO in the gas mixture on the Pt state. In the first step, reference HERFD-XANES spectra were acquired under model conditions to

https://doi.org/10.1021/acs.jpcc.5c01963
J. Phys. Chem. C XXXX, XXX, XXX−XXX

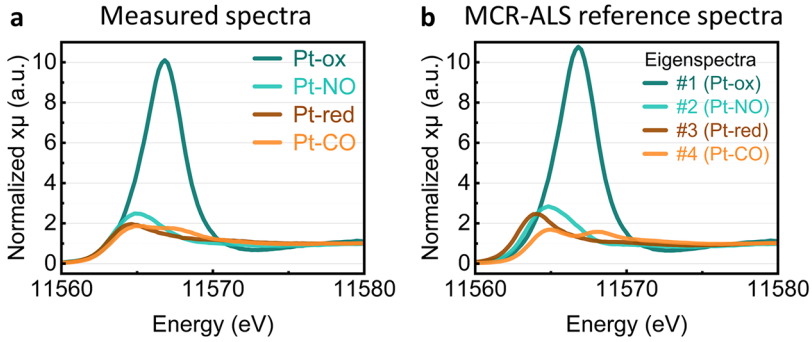

Figure 8. (a) Normalized HERFD-XANES reference spectra (Pt L3 edge) obtained experimentally on the differently treated 1.9% Pt/Al_2O_3 catalyst. (b) Spectra derived from the measured spectra using the multivariate curve resolution-alternating least-squares (MCR-ALS) algorithm. The designation in parentheses was given on the basis of the initial spectra from which the respective curves originated.

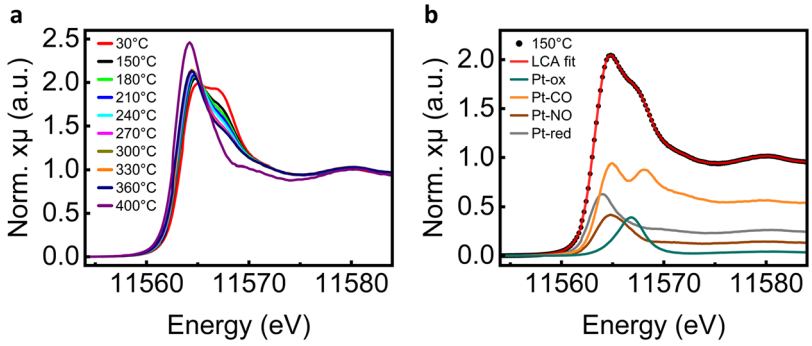

Figure 9. Normalized HERFD-XANES spectra (Pt L3 edge) recorded at the middle position of the 1.9% Pt/Al_2O_3 catalyst bed during the CO + NO reaction (2000 ppm CO/2000 ppm NO/He, WHSV = 25 000 L/($g_{noble\ metal}$ h)) (a) and the selected LCA together with the contribution of the LCA references for the HERFD-XANES measurement at 150 °C (b).

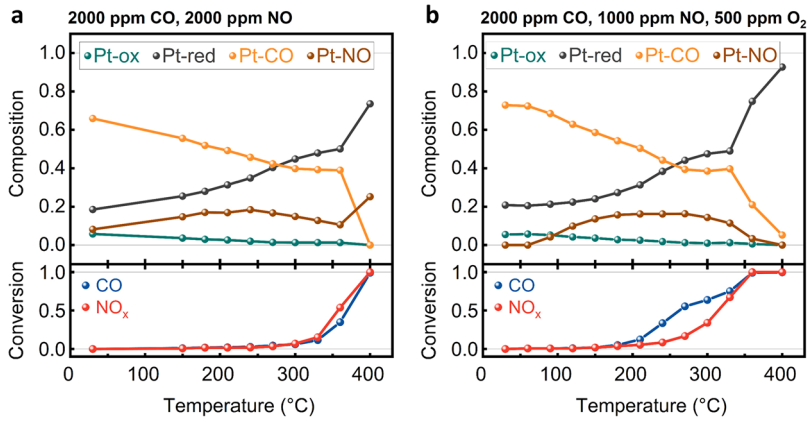

Figure 10. Chemical composition evolution of the prereduced 1.9% Pt/Al_2O_3 catalyst and gas conversions during the CO + NO (a) and the CO + NO + O_2 (b) reaction (WHSV = 25 000 L/($g_{noble\ metal}$ h). The chemical composition was obtained from HERFD-XANES LCA by using the calculated MCR-ALS reference spectra. The HERFD-XANES measurements were performed after a stabilization time of 30 min at each temperature step to ensure steady-state conditions.

identify the spectral features caused by the interaction with each gas component. A similarly prepared Pt/Al_2O_3 catalyst with a slightly higher noble metal loading of 1.9 wt % was selected in order to increase the fluorescence signal and therefore improve the data quality. To obtain defined reference spectra (Pt-ox, Pt-CO, Pt-NO, Pt-red), the sample was prereduced in a H_2-containing atmosphere at 500 °C before cooling to room temperature and dosing reactive gases (O_2, CO, NO, H_2). A more detailed overview on the applied conditions and on the data treatment is given in the Experimental Section. Figure 8a displays the recorded reference spectra after normalization.

The experimental HERFD-XANES spectra in Figure 8a show some similarities between metallic Pt (Pt-red), Pt-NO, and Pt-CO components in terms of white line intensity and position. In contrast, a significantly higher white line and a slight shift toward higher energies were observed for the Pt-ox state. In agreement with the literature,[47] a pronounced double-peak feature was detected for Pt-CO that can be attributed to linearly adsorbed CO on Pt.[24] This characteristic shape allowed distinguishing between Pt-red and Pt-CO species.

https://doi.org/10.1021/acs.jpcc.5c01963
J. Phys. Chem. C XXXX, XXX, XXX−XXX

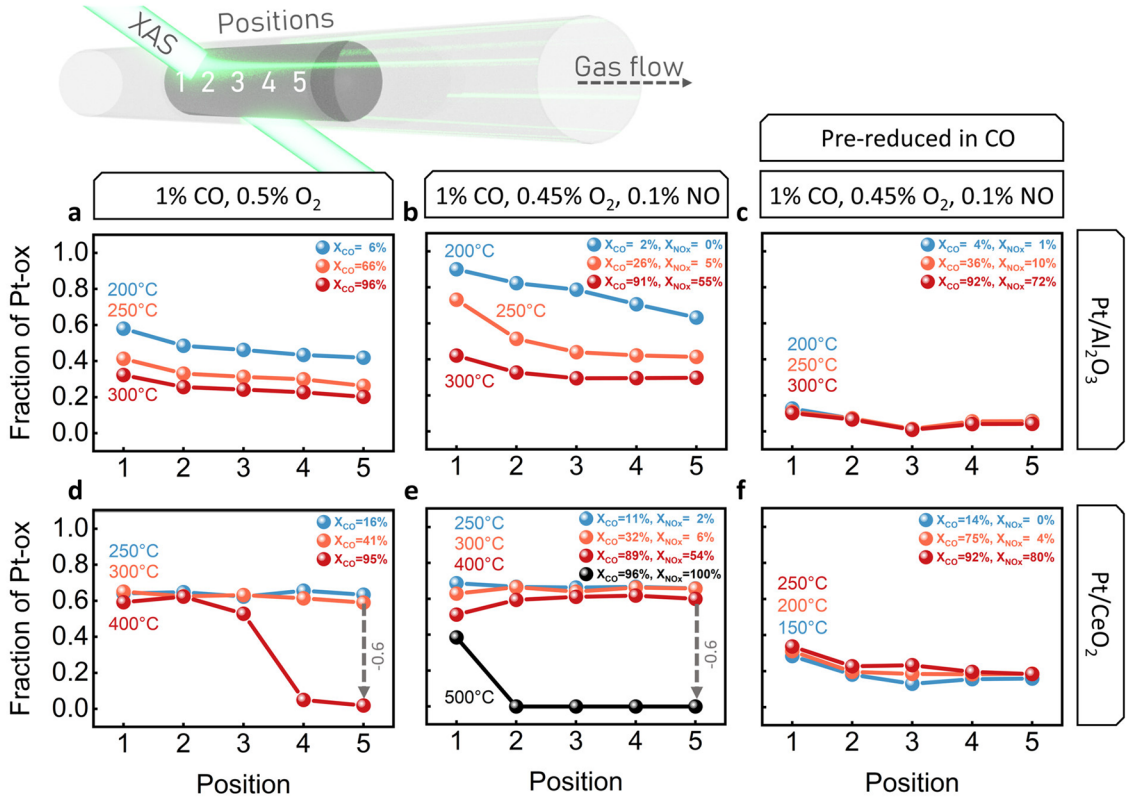

Figure 11. Spatially resolved evolution of the Pt-ox fraction for 1.0% Pt/Al_2O_3 (a–c) and 1.0% Pt/CeO_2 (d–f) for selected temperatures with low, medium, and high CO conversion. The results were derived from LCA of the XANES spectra recorded at five different positions. Position 1 represents the start and position 5 the end of the catalyst-packed beds. The respective total conversions of CO and NO are embedded within the figures.

The HERFD-XANES reference spectrum of Pt-NO was almost identical to that of Pt, only with a slightly higher white line intensity. This is in agreement with the oxidizing effect of NO on Pt, observed by *operando* XANES measurements (Figure 6a,b,d,e).

To verify that the measured reference spectra (Figure 8a) are sufficient to describe the evolution of Pt during the CO + O_2 + NO reaction, two experiments under stoichiometric conditions in the absence/presence of O_2 were conducted on the prereduced 1.9% Pt/Al_2O_3 catalyst. On the basis of the measured reference spectra (Figure 8a) in combination with HERFD-XANES data recorded during both experiments (e.g., Figure 9a for the CO/NO reaction), a multivariate curve resolution-alternating least-squares (MCR-ALS) analysis was performed. According to the MCR-ALS analysis, four eigenspectra (Figure 8b) were identified that exhibit strong similarities to the measured references. Since the calculated eigenspectra could be attributed to the respective Pt states, these were used as references for the LCA of both HERFD-XANES experiments, as shown in Figure 9b for one selected condition. Further LCA results are reported in the ESI (Figures S26 and S27).

According to the LCA results, the prereduced Pt/Al_2O_3 catalyst was mostly covered by CO at room temperature for both selected conditions (Figure 10a,b). Furthermore, only minor contributions of the Pt-ox and Pt-red components were observed. With rising temperature, adsorbed CO was slowly replaced by NO, as shown by the growing fraction of the Pt-NO contribution prior to the reaction onset. With increasing the CO and NO conversion, the Pt-CO and Pt-NO share gradually decreases in favor of metallic Pt. In contrast to the oxygen-free conditions (Figure 10a), the fraction of Pt-NO remained constant under CO + O_2 + NO atmosphere (Figure 10b) until significant NO conversion was observed at 270 °C. Consistent with the trends in the CO and NO conversion (Figure 2), the evolution of Pt-NO share confirmed the preferential participation of oxygen in the CO oxidation reaction at lower temperatures over NO. Only above 270 °C, when most of O_2 was consumed, a decrease in the fraction of Pt-NO was observed.

The LCA results also clearly indicate that even for a CO/NO ratio of 1 (Figure 10a), the contribution of the Pt-CO reference is at least a factor of 2 higher than that of Pt-NO. Furthermore, a maximum contribution of 0.2 was determined for the Pt-NO reference over the entire reaction range. Considering that the gas mixture selected for the experiments in Figure 6 contains 10 times more CO than NO (1% CO; 1000 ppm NO), it can be concluded that the contribution of Pt-NO plays only a minor role for the LCA of the conducted spatially resolved *operando* XAS investigations. Therefore, the Pt-NO species was neglected for the LCA depicted in Figure 6. After the contribution of the Pt-NO species to the overall fit is revealed and quantified, the spatially resolved evolution of Pt along the catalyst bed is discussed in more detail.

Spatial Evolution of the Pt Structure during Reaction. In the following step, XANES data recorded at different axial positions of the quartz capillary microreactor were analyzed for a variety of temperatures between 150 and 500 °C, at which low (≈ 10%), medium (≈ 50%), and high (≈ 95%) CO

https://doi.org/10.1021/acs.jpcc.5c01963
J. Phys. Chem. C XXXX, XXX, XXX−XXX

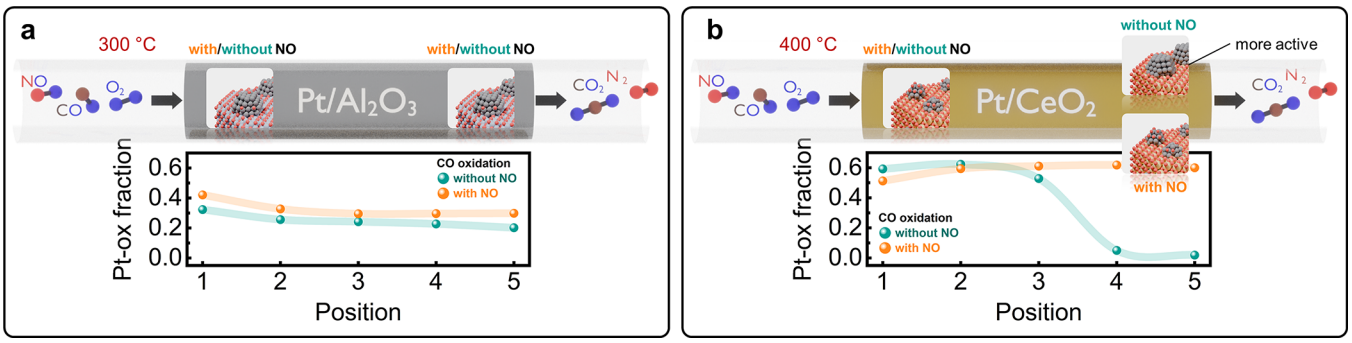

Figure 12. Schematic representation of the impact of NO on the reduction behavior of Pt-based catalysts under close-to-stoichiometric conditions, derived from the spatially resolved *operando* XAS. In particular, NO delayed the reduction of Pt particles in Pt/Al_2O_3 (a) and the formation of active clusters in Pt/CeO_2 (b). Furthermore, the reduction process was found to start at the end of the catalyst bed before propagating upstream at elevated temperatures.

conversion were observed. The spatially resolved fractions of Pt-ox derived from the LCA results are depicted in Figure 11.

At all selected temperatures (200−300 °C) for the Pt/Al_2O_3 catalyst (Figure 11a,b), a decreasing Pt oxidation state was observed downstream during CO oxidation independent of the presence of NO. With increasing temperature of the ongoing CO + O_2 reaction, a uniform decline in the Pt-ox fraction was observed at all positions in the catalyst bed. The addition of NO led to an increase in the Pt-ox contribution along the catalyst bed, indicating a shift in the Pt reduction to higher temperatures and net-reducing conditions. A similar conclusion can be drawn from the LCA based on the temperature-dependent evolution of the metallic Pt reference (Pt-red in Figures S17 and S18). This observation underlines that the variation in the Pt-ox fraction is related to changes in the Pt particle size.

In contrast, the spatially resolved investigation of the Pt/CeO_2 catalyst for the identical gas mixture (Figure 11d) showed no spatial gradients at low and medium CO conversion values. At high CO conversion (T = 400 °C), a strong gradient in the Pt-ox fraction was observed along the catalyst bed. In this case, the noble metal in the downstream part of the catalyst (positions 4 and 5) became strongly reduced, while for upstream positions (positions 1−3), the Pt-ox fraction remained unchanged. Such an evolution indicates the progression of the reaction zone toward position 1 with rising temperature,[36] leading, under slightly rich conditions, to a reductive gas atmosphere at the end of the catalyst bed (Figure S20). On the contrary, the presence of oxygen in the gas phase at upstream positions suppresses the reduction of Pt.

When NO was added to the gas mixture (Figure 11e), the downstream reduction/particle formation was not observed anymore for Pt/CeO_2 at 250−400 °C, resulting in a rather homogeneous catalyst state along the bed. Similarly to the case for O_2 during CO oxidation, the presence of NO delayed Pt reduction and the *in situ* formation of active Pt clusters on CeO_2 (Figures S20 and S21), which can explain the rather low overall activity obtained over highly dispersed Pt/CeO_2, as discussed above (Figure 2). Nonetheless, with the progression of the CO + NO + O_2 reaction, a reduction of Pt-ox was observed above 400 °C at the downstream positions (pos. 2−5).

While comparing the differences in the gradient formation for Pt/Al_2O_3 and Pt/CeO_2 at lower to medium conversion values, a less pronounced gradient in the Pt oxidation state is observed for Pt/CeO_2 (Figure 11e,f) than for Pt/Al_2O_3. Such behavior can be potentially explained by the redox properties of CeO_2 and the contribution of the Mars-van Krevelen mechanism to the overall activity for Pt/CeO_2. In this case, lattice oxygen of CeO_2 is also involved in the CO oxidation reaction, in addition to oxygen adsorbed on Pt. As reported in the literature,[47,51] the Mars-van Krevelen route is dominant compared to the Langmuir−Hinshelwood pathway in the low-temperature range, while both mechanisms contribute to the overall reaction at elevated temperatures.

After prereduction in 1% CO/He at 400 °C, in both catalysts Pt was present in a strongly reduced state, which did not change with increasing temperature and conversion (Figure 11c,f). The overall noble metal oxidation state inPt/Al_2O_3 was slightly lower than that in Pt/CeO_2. In agreement with the EXAFS analysis results, this hints at a larger Pt particle size on Al_2O_3 than on Pt/CeO_2. In terms of spatial gradients, Pt at the beginning of the catalyst bed (pos. 1) was more oxidized than at the downstream positions in the case of Pt/CeO_2. Considering that these changes are not observed in the EXAFS data recorded after the prereduction (Figure 4), a downstream decrease in the gas phase O_2 content with progressing reaction might explain the detected trends.

In conclusion, spatially resolved *operando* XAS results revealed the decisive impact of NO on the reduction behavior of Pt-based catalysts under close-to-stoichiometric conditions. More precisely, the reduction of Pt particles in Pt/Al_2O_3 and the formation of active Pt clusters in highly dispersed Pt/CeO_2 were shifted to higher temperatures in the presence of NO. According to spatially resolved *operando* XAS, the reduction process was initiated at the end of the catalyst bed, as visualized in Figure 12, and propagated upstream with increasing temperature. However, the influence of NO on the Pt particle formation and reduction behavior could be minimized by applying a reductive treatment prior to the catalytic cycle.

■ CONCLUSIONS

In this study, the influence of NO on the CO oxidation reaction under close-to-stoichiometric conditions was studied for Pt/CeO_2 and Pt/Al_2O_3 using complementary *in situ*/*operando* XAS, DRIFTS, and HERFD-XANES. Although Pt was dispersed as single atoms/clusters on CeO_2, Pt nanoparticles with an average size of about 1.3 nm were observed in Pt/Al_2O_3. For both catalysts, the presence of NO shifted the onset of the CO oxidation reaction to higher temperatures. Additionally, CO was shown to preferentially be oxidized by

https://doi.org/10.1021/acs.jpcc.5c01963
J. Phys. Chem. C XXXX, XXX, XXX−XXX

O_2 rather than NO below 300 °C. With the as-prepared samples, a higher catalytic performance was observed for Pt/Al_2O_3 compared to Pt/CeO_2 in the presence as well as in the absence of NO. Catalyst activation was obtained for both Pt-based samples by applying a reductive treatment. Hereby, the impact of the catalyst prereduction was more pronounced for Pt/CeO_2 than for Pt/Al_2O_3. Competitive adsorption of CO and NO, uncovered by *in situ* DRIFTS, is probably the cause for the delayed ignition of the CO oxidation reaction over Pt-based catalysts in the presence of NO. By performing complementary *operando* HERFD-XANES experiments, we could further quantify the fraction of different Pt species. Even for equal CO/NO ratios, at least a two-times higher contribution of Pt-CO adsorbates in comparison to Pt-NO was observed for Pt/Al_2O_3, underlining the favored adsorption of CO on the Pt surface. Spatially resolved *operando* XAS investigations revealed the crucial role of NO on the reduction behavior of Pt under reaction conditions. Under net-reducing conditions, cluster formation for Pt/CeO_2 and particle reduction for Pt/Al_2O_3 were found to start at the end of the catalyst bed and to progress upstream with increasing temperature. However, the noble metal reduction behavior was slowed down in the presence of NO for both catalysts. For the highly dispersed Pt/CeO_2 catalyst, the limited *in situ* Pt cluster formation resulted in a gradient along the catalyst bed with the beginning position being more oxidized. Such structural evolution may also explain the rather low overall activity of this catalyst in the as-prepared state. The negative impact of NO on the formation of active Pt clusters could be overcome by applying a reductive treatment, resulting in a homogeneous, reduced Pt state along the catalyst bed and therefore improved catalytic performance.

■ ASSOCIATED CONTENT

Data Availability Statement

The data used for the results in this manuscript is available at the KITopen repository. DOI: 10.35097/sqp2keataytwhzx1 Furthermore, the HERFD-XANES raw-data will also be available at the ESRF website under DOI: 10.15151/ESRF-ES-1312118706. Processed XANES and HERFD-XANES data are available at the RefXAS database (https://doi.org/10.1107/S1600577524006751).

Supporting Information

The Supporting Information is available free of charge at https://pubs.acs.org/doi/10.1021/acs.jpcc.5c01963.

Additional information on the *ex situ* characterization, EXAFS fitting, LCA results for *operando* XAS and HERFD-XANES, as well as *in situ* DRIFTS experiments (PDF)

■ AUTHOR INFORMATION

Corresponding Author

Jan-Dierk Grunwaldt − *Institute for Chemical Technology and Polymer Chemistry (ITCP), Karlsruhe Institute of Technology (KIT), 76131 Karlsruhe, Germany; Institute of Catalysis Research and Technology (IKFT), Karlsruhe Institute of Technology (KIT), 76344 Eggenstein-Leopoldshafen, Germany;* orcid.org/0000-0003-3606-0956; Email: grunwaldt@kit.edu

Authors

Daria Gashnikova − *Institute for Chemical Technology and Polymer Chemistry (ITCP), Karlsruhe Institute of Technology (KIT), 76131 Karlsruhe, Germany;* orcid.org/0009-0007-3492-7997

Samuel Struzek − *Institute for Chemical Technology and Polymer Chemistry (ITCP), Karlsruhe Institute of Technology (KIT), 76131 Karlsruhe, Germany*

Florian Maurer − *Institute for Chemical Technology and Polymer Chemistry (ITCP), Karlsruhe Institute of Technology (KIT), 76131 Karlsruhe, Germany;* orcid.org/0000-0002-3307-4132

Miriam R. Bauer − *Institute for Chemical Technology and Polymer Chemistry (ITCP), Karlsruhe Institute of Technology (KIT), 76131 Karlsruhe, Germany*

Carina B. Maliakkal − *Institute of Nanotechnology (INT), Karlsruhe Institute of Technology (KIT), 76344 Eggenstein-Leopoldshafen, Germany*

Christian Kübel − *Institute of Nanotechnology (INT) and Karlsruhe Nano Micro Facility (KNMFi), Karlsruhe Institute of Technology (KIT), 76344 Eggenstein-Leopoldshafen, Germany; Department of Materials and Earth Sciences, Technical University Darmstadt (TUDa), 64287 Darmstadt, Germany;* orcid.org/0000-0001-5701-4006

Maria Casapu − *Institute for Chemical Technology and Polymer Chemistry (ITCP), Karlsruhe Institute of Technology (KIT), 76131 Karlsruhe, Germany;* orcid.org/0000-0002-8755-9856

Complete contact information is available at: https://pubs.acs.org/10.1021/acs.jpcc.5c01963

Author Contributions

#D.G. and S.S. shared first authorship.

Notes

The authors declare no competing financial interest.

■ ACKNOWLEDGMENTS

This study was funded by the Deutsche Forschungsgemeinschaft (DFG, German Research Foundation)—SFB 1441—Project-ID 426888090 (projects A3/B1, B2, B3, C4). D.G. further acknowledges the "Fonds der Chemischen Industrie" (FCI) of the Verband der Chemischen Industrie e.V. (VCI) for financial support during her Ph.D. studies. The authors acknowledge the European Synchrotron Radiation Facility (ESRF) for provision of synchrotron radiation facilities under proposal number CH-6752 and we would like to thank B. Detlefs and T. Bohdan for assistance in using beamline ID26. Furthermore, the authors thank the Deutsches Elektronen-Synchrotron (DESY), a member of the Helmholtz Association HGF, for beamtime at the P65 beamline (proposal number: I-20210886) and the ErUM-Pro program of the German Federal Ministry of Education and Research (BMBF) for supporting the infrastructure at DESY. Additionally, we acknowledge E. Welter for kind assistance during the experiments. Electron microscopy was supported by the Karlsruhe Nano Micro Facility (KNMFi), a Helmholtz Research Infrastructure at KIT. T. Bergfeldt (IAM-AWP, KIT) is acknowledged for ICP-OES analysis and A. Deutsch (ITCP, KIT) for BET measurements. The authors thank J. Czechowsky (ITCP, KIT) for providing the reference Pt/Al_2O_3 sample used for the HERFD-XANES measurements as well as Simon Barth for his help regarding the DRIFTS measurements. The authors thank

DAPHNE4NFDI (DFG project under project number 460248799) as well as further NFDI-consortia (NFDI4Cat, FAIRMAT, and NFDI4Chem) for fruitful discussion and valuable input for implementing FAIR data principles in this work.

REFERENCES

(1) Jokl, M. V. The Danger of Toxic Substances. *Acta Polytech.*. **2002**, *42*13−21. DOI: 10.14311/346
(2) Xu, Z.; Li, Y.; Lin, Y.; Zhu, T. A review of the catalysts used in the reduction of NO by CO for gas purification. *Environ. Sci. Pollut. Res.* **2020**, *27*, 6723−6748.
(3) Lott, P.; Casapu, M.; Grunwaldt, J.-D.; Deutschmann, O. A review on exhaust gas after-treatment of lean-burn natural gas engines−from fundamentals to application. *Appl. Catal., B* **2024**, *340*, No. 123241.
(4) Datye, A. K.; Votsmeier, M. Opportunities and challenges in the development of advanced materials for emission control catalysts. *Nat. Mater.* **2021**, *20*, 1049−1059.
(5) Rood, S.; Eslava, S.; Manigrasso, A.; Bannister, C. Recent advances in gasoline three-way catalyst formulation: A review. *Proc. Inst. Mech. Eng., Part D* **2020**, *234*, 936−949.
(6) Deutschmann, O.; Grunwaldt, J.-D. Exhaust gas aftertreatment in mobile systems: status, challenges, and perspectives. *Chem. Ing. Tech.* **2013**, *85*, 595−617.
(7) Dubbe, H.; Bühner, F.; Eigenberger, G.; Nieken, U. Hysteresis phenomena on platinum and palladium-based diesel oxidation catalysts (DOCs). *Emiss. Control Sci. Technol.* **2016**, *2*, 137−144.
(8) Etzold, B. J.; Krewer, U.; Thiele, S.; Dreizler, A.; Klemm, E.; Turek, T. Understanding the activity transport nexus in water and CO_2 electrolysis: State of the art, challenges and perspectives. *Chem. Eng. J.* **2021**, *424*, No. 130501.
(9) Liu, Y.; Wang, Q.; Zhang, J.; Ding, J.; Cheng, Y.; Wang, T.; Li, J.; Hu, F.; Yang, H. B.; Liu, B. Recent advances in carbon-supported noble-metal electrocatalysts for hydrogen evolution reaction: syntheses, structures, and properties. *Adv. Energy Mater.* **2022**, *12*, No. 2200928.
(10) Lan, X.; Wang, T. Highly selective catalysts for the hydrogenation of unsaturated aldehydes: a review. *ACS Catal.* **2020**, *10*, 2764−2790.
(11) Zhao, X.; Chang, Y.; Chen, W.-J.; Wu, Q.; Pan, X.; Chen, K.; Weng, B. Recent progress in Pd-based nanocatalysts for selective hydrogenation. *ACS Omega* **2022**, *7*, 17−31.
(12) Granger, P.; Dathy, C.; Lecomte, J.; Leclercq, L.; Prigent, M.; Mabilon, G.; Leclercq, G. Kinetics of the NO and CO reaction over platinum catalysts: I. Influence of the support. *J. Catal.* **1998**, *173*, 304−314.
(13) Srinivasan, A.; Depcik, C. Review of Chemical Reactions in the NO Reduction by CO on Platinum/Alumina Catalysts. *Surf. Rev. Lett.* **2012**, *19*, No. 1230001.
(14) Freysz, J.-L.; Saussey, J.; Lavalley, J.-C.; Bourges, P. In situ FTIR study of the NO+CO reaction on a silica-supported platinum catalyst at atmospheric pressure using a new pulse technique. *J. Catal.* **2001**, *197*, 131−138.
(15) Bell, A. T.; Lorimer, D. Reduction of NO by CO over a silica-supported platinum catalyst: Infrared and kinetic studies. *J. Catal.* **1979**, *59*, 223−238.
(16) Unland, M. L. Isocyanate intermediates in the reaction nitrogen monoxide+ carbon monoxide over a platinum/aluminum oxide catalyst. *J. Phys. Chem. A* **1973**, *77*, 1952−1956.
(17) Solymosi, F.; Sarkany, J.; Schauer, A. Study of the formation of Isocyanate surface complexes on Pt/Al_2O_3 catalysts. *J. Catal.* **1977**, *46*, 297−307.
(18) Di, M.; Schaefer, A.; Hemmingsson, F.; Bell, T.; Feng, Y.; Skoglundh, M.; Thompsett, D.; Carlsson, P.-A. Why nitrogen oxide inhibits CO oxidation over highly dispersed platinum ceria catalysts. *Catal. Today* **2024**, *426*, No. 114394.
(19) Newton, M. A.; Belver-Coldeira, C.; Martínez-Arias, A.; Fernández-García, M. Dynamic in situ observation of rapid size and shape change of supported Pd nanoparticles during CO/NO cycling. *Nat. Mater.* **2007**, *6*, 528−532.
(20) Dent, A. J.; Evans, J.; Fiddy, S. G.; Jyoti, B.; Newton, M. A.; Tromp, M. Rhodium dispersion during NO/CO conversions. *Angew. Chem., Int. Ed.* **2007**, *46*, 5356−5358.
(21) Sarma, B. B.; Grunwaldt, J.-D. Operando Spectroscopy to Understand Dynamic Structural Changes of Solid Catalysts. *Chimia* **2024**, *78*, 288−296.
(22) Weckhuysen, B. M. Determining the active site in a catalytic process: Operando spectroscopy is more than a buzzword. *Phys. Chem. Chem. Phys.* **2003**, *5*, 4351−4360.
(23) Bañares, M. A. Operando methodology: combination of in situ spectroscopy and simultaneous activity measurements under catalytic reaction conditions. *Catal. Today* **2005**, *100*, 71−77.
(24) Safonova, O. V.; Tromp, M.; van Bokhoven, J. A.; de Groot, F. M.; Evans, J.; Glatzel, P. Identification of CO adsorption sites in supported Pt catalysts using high-energy-resolution fluorescence detection X-ray spectroscopy. *J. Phys. Chem. B* **2006**, *110*, 16162−16164.
(25) Singh, J.; Nelson, R. C.; Vicente, B. C.; Scott, S. L.; van Bokhoven, J. A. Electronic structure of alumina-supported monometallic Pt and bimetallic PtSn catalysts under hydrogen and carbon monoxide environment. *Phys. Chem. Chem. Phys.* **2010**, *12*, 5668−5677.
(26) Maurer, F.; Gänzler, A.; Lott, P.; Betz, B.; Votsmeier, M.; Loridant, S.; Vernoux, P.; Murzin, V.; Bornmann, B.; Frahm, R.; Deutschmann, O.; Casapu, M.; Grunwaldt, J.-D. Spatiotemporal investigation of the temperature and structure of a Pt/CeO_2 oxidation catalyst for CO and hydrocarbon oxidation during pulse activation. *Ind. Eng. Chem. Res.* **2021**, *60*, 6662−6675.
(27) Urakawa, A.; Baiker, A. Space-resolved profiling relevant in heterogeneous catalysis. *Top. Catal.* **2009**, *52*, 1312−1322.
(28) Dann, E. K.; Gibson, E. K.; Catlow, C. R. A.; Celorrio, V.; Collier, P.; Eralp, T.; Amboage, M.; Hardacre, C.; Stere, C.; Kroner, A.; Raj, A.; Rogers, S.; Goguet, A.; Wells, P. P. Combined spatially resolved operando spectroscopy: New insights into kinetic oscillations of CO oxidation on $Pd/\gamma\text{-}Al_2O_3$. *J. Catal.* **2019**, *373*, 201−208.
(29) Gänzler, A. M.; Betz, B.; Baier-Stegmaier, S.; Belin, S.; Briois, V.; Votsmeier, M.; Casapu, M. Operando X-ray Absorption Spectroscopy Study During Conditioning of Pt-Based Catalysts and Its Implications for CO Oxidation. *J. Phys. Chem. C* **2020**, *124*, 20090−20100.
(30) Gänzler, A. M.; Casapu, M.; Vernoux, P.; Loridant, S.; Cadete Santos Aires, F. J.; Epicier, T.; Betz, B.; Hoyer, R.; Grunwaldt, J.-D. Tuning the structure of platinum particles on ceria in situ for enhancing the catalytic performance of exhaust gas catalysts. *Angew. Chem., Int. Ed.* **2017**, *56*, 13078−13082.
(31) Maurer, F.; Jelic, J.; Wang, J.; Gänzler, A.; Dolcet, P.; Wöll, C.; Wang, Y.; Studt, F.; Casapu, M.; Grunwaldt, J.-D. Tracking the formation, fate and consequence for catalytic activity of Pt single sites on CeO_2. *Nat. Catal.* **2020**, *3*, 824−833.
(32) Eggart, D.; Huang, X.; Zimina, A.; Yang, J.; Pan, Y.; Pan, X.; Grunwaldt, J.-D. Operando XAS study of Pt-doped CeO_2 for the nonoxidative conversion of methane. *ACS Catal.* **2022**, *12*, 3897−3908.
(33) Brunauer, S.; Emmett, P. H.; Teller, E. Adsorption of gases in multimolecular layers. *J. Am. Chem. Soc.* **1938**, *60*, 309−319.
(34) Grunwaldt, J.-D.; Caravati, M.; Hannemann, S.; Baiker, A. X-ray absorption spectroscopy under reaction conditions: suitability of different reaction cells for combined catalyst characterization and time-resolved studies. *Phys. Chem. Chem. Phys.* **2004**, *6*, 3037−3047.
(35) Clausen, B. S.; Steffensen, G.; Fabius, B.; Villadsen, J.; Feidenhans, R.; Topsøe, H. In situ cell for combined XRD and on-line catalysis tests: Studies of Cu-based water gas shift and methanol catalysts. *J. Catal.* **1991**, *132*, 524−535.
(36) Gänzler, A. M.; Casapu, M.; Boubnov, A.; Müller, O.; Conrad, S.; Lichtenberg, H.; Frahm, R.; Grunwaldt, J.-D. Operando spatially

and time-resolved X-ray absorption spectroscopy and infrared thermography during oscillatory CO oxidation. *J. Catal.* **2015**, *328*, 216−224.
(37) Chatterjee, D.; Deutschmann, O.; Warnatz, J. Detailed surface reaction mechanism in a three-way catalyst. *Faraday Discuss* **2001**, *119*, 371−384.
(38) Ravel, B.; Newville, M. ATHENA, ARTEMIS, HEPHAESTUS: data analysis for X-ray absorption spectroscopy using IFEFFIT. *J. Synchrotron Radiat.* **2005**, *12*, 537−541.
(39) Landrot, G. FASTOSH: A Software to Process XAFS Data for Geochemical & Environmental Applications. *Goldschmidt Abstracts* **2018**, *1402*, 1.
(40) Glatzel, P.; Harris, A.; Marion, P.; Sikora, M.; Weng, T.-C.; Guilloud, C.; Lafuerza, S.; Rovezzi, M.; Detlefs, B.; Ducotté, L. The five-analyzer point-to-point scanning crystal spectrometer at ESRF ID26. *J. Synchrotron Radiat.* **2021**, *28*, 362−371.
(41) Gashnikova, D.; Maurer, F.; Sauter, E.; Bernart, S.; Jelic, J.; Dolcet, P.; Maliakkal, C. B.; Wang, Y.; Wöll, C.; Studt, F.; Kübel, C.; Casapu, M.; Grunwaldt, J.-D. Highly Active Oxidation Catalysts through Confining Pd Clusters on CeO_2 Nano-Islands. *Angew. Chem., Int. Ed.* **2024**, *63*, No. e202408511.
(42) Jones, J.; Xiong, H.; DeLaRiva, A. T.; Peterson, E. J.; Pham, H.; Challa, S. R.; Qi, G.; Oh, S.; Wiebenga, M. H.; Pereira Hernández, X. I.; Wang, Y.; Datye, A. K. Thermally stable single-atom platinum-on-ceria catalysts via atom trapping. *Science* **2016**, *353*, 150−154.
(43) Nie, L.; Mei, D.; Xiong, H.; Peng, B.; Ren, Z.; Hernandez, X. I. P.; DeLaRiva, A.; Wang, M.; Engelhard, M. H.; Kovarik, L.; Datye, A. K.; Wang, Y. Activation of surface lattice oxygen in single-atom Pt/CeO_2 for low-temperature CO oxidation. *Science* **2017**, *358*, 1419−1423.
(44) Lambert, R.; Comrie, C. The Oxidation of CO by NO on Pt (111) and Pt (110). *Surf. Sci.* **1974**, *46*, 61−80.
(45) Zhang, Z.; Tian, J.; Lu, Y.; Yang, S.; Jiang, D.; Huang, W.; Li, Y.; Hong, J.; Hoffman, A. S.; Bare, S. R.; Engelhard, M. H.; Datye, A. K.; Wang, Y. Memory-dictated dynamics of single-atom Pt on CeO_2 for CO oxidation. *Nat. Commun.* **2023**, *14*, No. 2664.
(46) Kunwar, D.; Zhou, S.; DeLaRiva, A.; et al. Stabilizing high metal loadings of thermally stable platinum single atoms on an industrial catalyst support. *ACS Catal.* **2019**, *9*, 3978−3990.
(47) Gänzler, A. M.; Casapu, M.; Doronkin, D. E.; Maurer, F.; Lott, P.; Glatzel, P.; Votsmeier, M.; Deutschmann, O.; Grunwaldt, J.-D. Unravelling the different reaction pathways for low temperature CO oxidation on Pt/CeO_2 and Pt/Al_2O_3 by spatially resolved structure−activity correlations. *J. Phys. Chem. Lett.* **2019**, *10*, 7698−7705.
(48) Mergler, Y.; Nieuwenhuys, B. NO Reduction by CO over Pt/Al_2O_3 and Pt/CeO_x/Al_2O_3: Oscillations and Deactivation. *J. Catal.* **1996**, *161*, 292−303.
(49) Yaldram, K.; Khan, M. NO-CO reaction on square and hexagonal surfaces: A Monte Carlo simulation. *J. Catal.* **1991**, *131*, 369−377.
(50) Granger, P.; Praliaud, H.; Billy, J.; Leclercq, L.; Leclercq, G. Infrared investigation of the transformation of NO over supported Pt- and Rh-based three-way catalysts. *Surf. Interface Anal.* **2002**, *34*, 92−96.
(51) Cargnello, M.; Doan-Nguyen, V. V.; Gordon, T. R.; Diaz, R. E.; Stach, E. A.; Gorte, R. J.; Fornasiero, P.; Murray, C. B. Control of metal nanocrystal size reveals metal-support interface role for ceria catalysts. *Science* **2013**, *341*, 771−773.
(52) Muravev, V.; Simons, J. F.; Parastaev, A.; Verheijen, M. A.; Struijs, J. J.; Kosinov, N.; Hensen, E. J. Operando spectroscopy unveils the catalytic role of different palladium oxidation states in CO oxidation on Pd/CeO_2 catalysts. *Angew. Chem., Int. Ed.* **2022**, *61*, No. e202200434.
(53) Gänzler, A.; Lichtenberg, H.; Frenkel, A.; Casapu, M.; Boubnov, A.; Wang, D.; Grunwaldt, J.-D. Using combined XAS/DRIFTS to study CO/NO Oxidation over Pt/Al_2O_3 catalysts. *J. Phys.: Conf. Ser.* **2016**, *712*, No. 012045.
(54) Marinković, N. S.; Sasaki, K.; Adžić, R. R. Nanoparticle size evaluation of catalysts by EXAFS: Advantages and limitations. *Zast. Mater.* **2016**, *57*, 101−109.
(55) Bourane, A.; Bianchi, D. Oxidation of CO on a Pt/Al_2O_3 catalyst: From the surface elementary steps to light-off tests: I. Kinetic study of the oxidation of the linear CO species. *J. Catal.* **2001**, *202*, 34−44.
(56) Vayssilov, G. N.; Lykhach, Y.; Migani, A.; Staudt, T.; Petrova, G. P.; Tsud, N.; Skála, T.; Bruix, A.; Illas, F.; Prince, K. C.; Matolín, V.; Neyman, K. M.; Libuda, J. Support nanostructure boosts oxygen transfer to catalytically active platinum nanoparticles. *Nat. Mater.* **2011**, *10*, 310−315.
(57) Lykhach, Y.; Kozlov, S. M.; Skála, T.; Tovt, A.; Stetsovych, V.; Tsud, N.; Dvořák, F.; Johánek, V.; Neitzel, A.; Mysliveček, J.; Fabris, S.; Matolín, V.; Neyman, K. M.; Libuda, J. Counting electrons on supported nanoparticles. *Nat. Mater.* **2016**, *15*, 284−288.
(58) Castoldi, L.; Lietti, L.; Bonzi, R.; Artioli, N.; Forzatti, P.; Morandi, S.; Ghiotti, G. The NO_x Reduction by CO on a Pt- K/Al_2O_3 Lean NO_x Trap Catalyst. *J. Phys. Chem. C* **2011**, *115*, 1277−1286.
(59) Mihaylov, M. Y.; Ivanova, E. Z.; Aleksandrov, H. A.; Petkov, P. S.; Vayssilov, G. N.; Hadjiivanov, K. I. FTIR and density functional study of NO interaction with reduced ceria: Identification of N_3^- and NO^{2-} as new intermediates in NO conversion. *Appl. Catal., B* **2015**, *176−177*, 107−119.
(60) Haneda, M.; Morita, T.; Nagao, Y.; Kintaichi, Y.; Hamada, H. CeO_2-ZrO_2 binary oxides for NO_x removal by sorption. *Phys. Chem. Chem. Phys.* **2001**, *3*, 4696−4700.
(61) Azambre, B.; Atribak, I.; Bueno-Lopez, A.; García-García, A. Probing the Surface of Ceria- Zirconia Catalysts Using NO_x Adsorption/Desorption: A First Step Toward the Investigation of Crystallite Heterogeneity. *J. Phys. Chem. C* **2010**, *114*, 13300−13312.
(62) Liu, N.; Chen, X.; Zhang, J.; Schwank, J. W. DRIFTS study of photo-assisted catalytic CO + NO redox reaction over CuO/CeO_2-TiO_2. *Catal. Today* **2015**, *258*, 139−147.
(63) Vayssilov, G. N.; Mihaylov, M.; Petkov, P. S.; Hadjiivanov, K. I.; Neyman, K. M. Reassignment of the vibrational spectra of carbonates, formates, and related surface species on ceria: a combined density functional and infrared spectroscopy investigation. *J. Phys. Chem. C* **2011**, *115*, 23435−23454.
(64) Meunier, F. C.; Tibiletti, D.; Goguet, A.; Reid, D.; Burch, R. On the reactivity of carbonate species on a Pt/CeO_2 catalyst under various reaction atmospheres: Application of the isotopic exchange technique. *Appl. Catal., A* **2005**, *289*, 104−112.
(65) Meunier, F. C. Relevance of IR spectroscopy of adsorbed CO for the characterization of heterogeneous catalysts containing isolated atoms. *J. Phys. Chem. C* **2021**, *125*, 21810−21823.
(66) Resasco, J.; DeRita, L.; Dai, S.; Chada, J. P.; Xu, M.; Yan, X.; Finzel, J.; Hanukovich, S.; Hoffman, A. S.; Graham, G. W.; Bare, S. R.; Pan, X.; Christopher, P. Uniformity is key in defining structure−function relationships for atomically dispersed metal catalysts: the case of Pt/CeO_2. *J. Am. Chem. Soc.* **2020**, *142*, 169−184.
(67) Agrawal, V. K.; Trenary, M. An infrared study of NO adsorption at defect sites on Pt (111). *Surf. Sci.* **1991**, *259*, 116−128.
(68) Newton, M. A.; Ferri, D.; Smolentsev, G.; Marchionni, V.; Nachtegaal, M. Room-temperature carbon monoxide oxidation by oxygen over Pt/Al_2O_3 mediated by reactive platinum carbonates. *Nat. Commun.* **2015**, *6*, No. 8675.
(69) Chilukoti, S.; Gao, F.; Anderson, B. G.; Niemantsverdriet, J. H.; Garland, M. Pure component spectral analysis of surface adsorbed species measured under real conditions. BTEM-DRIFTS study of CO and NO reaction over a Pd/γ-Al_2O_3 catalyst. *Phys. Chem. Chem. Phys.* **2008**, *10*, 5510−5520.
(70) Sarma, B. B.; Jelic, J.; Neukum, D.; Doronkin, D. E.; Huang, X.; Studt, F.; Grunwaldt, J.-D. Tracking and understanding dynamics of atoms and clusters of late transition metals with in-situ DRIFT and XAS spectroscopy assisted by DFT. *J. Phys. Chem. C* **2023**, *127*, 3032−3046.
(71) Mitchell, M. B.Fundamentals and Applications of Diffuse Reflectance Infrared Fourier Transform (DRIFT) Spectroscopy.

https://doi.org/10.1021/acs.jpcc.5c01963
J. Phys. Chem. C XXXX, XXX, XXX−XXX

Structure−Property Relations in Polymers, Advances in Chemistry; American Chemical Society, 1993; Vol. *236*, pp 351−375.
(72) Ivanova, E.; Mihaylov, M.; Thibault-Starzyk, F.; Daturi, M.; Hadjiivanov, K. FTIR spectroscopy study of CO and NO adsorption and co-adsorption on Pt/TiO_2. *J. Mol. Catal. A: Chem.* **2007**, *274*, 179−184.
(73) Ohno, T.; Tanaka, E.; Hatayama, F.; Toda, Y.; Miyata, H. Promoting effect of Pt addition to V_2O_5/ZrO_2 catalyst on reduction of NO by C_3H_6. *Catal. Lett.* **2001**, *77*, 183−187.
(74) Primet, M.; Basset, J.; Garbowski, E.; Mathieu, M. Influence of metal particle size on the chemisorption properties of supported platinum. Analogy with cluster compounds. *J. Am. Chem. Soc.* **1975**, *97*, 3655−3659.
(75) Maurer, F.; Beck, A.; Jelic, J.; Wang, W.; Mangold, S.; Stehle, M.; Wang, D.; Dolcet, P.; Gänzler, A. M.; Kübel, C.; et al. Surface noble metal concentration on ceria as a key descriptor for efficient catalytic CO oxidation. *ACS Catal.* **2022**, *12*, 2473−2486.
(76) Dolcet, P.; Maurer, F.; Casapu, M.; Grunwaldt, J.-D. Insights into the Structural Dynamics of Pt/CeO_2 Single-Site Catalysts during CO Oxidation. *Catalysts* **2021**, *11*, No. 617.
(77) Zhou, Y.; Doronkin, D. E.; Zhao, Z.; Plessow, P. N.; Jelic, J.; Detlefs, B.; Pruessmann, T.; Studt, F.; Grunwaldt, J.-D. Photothermal catalysis over nonplasmonic Pt/TiO_2 studied by operando HERFD-XANES, resonant XES, and DRIFTS. *ACS Catal.* **2018**, *8*, 11398−11406.
(78) Glatzel, P.; Weng, T.-C.; Kvashnina, K.; Swarbrick, J.; Sikora, M.; Gallo, E.; Smolentsev, N.; Mori, R. A. Reflections on hard X-ray photon-in/photon-out spectroscopy for electronic structure studies. *J. Electron Spectrosc. Relat. Phenom.* **2013**, *188*, 17−25.

https://doi.org/10.1021/acs.jpcc.5c01963
J. Phys. Chem. C XXXX, XXX, XXX−XXX